

Susceptibility and Conductivity MRI

Jingwen Yao

M229 Advanced Topics in MRI

May 25, 2023

Outline

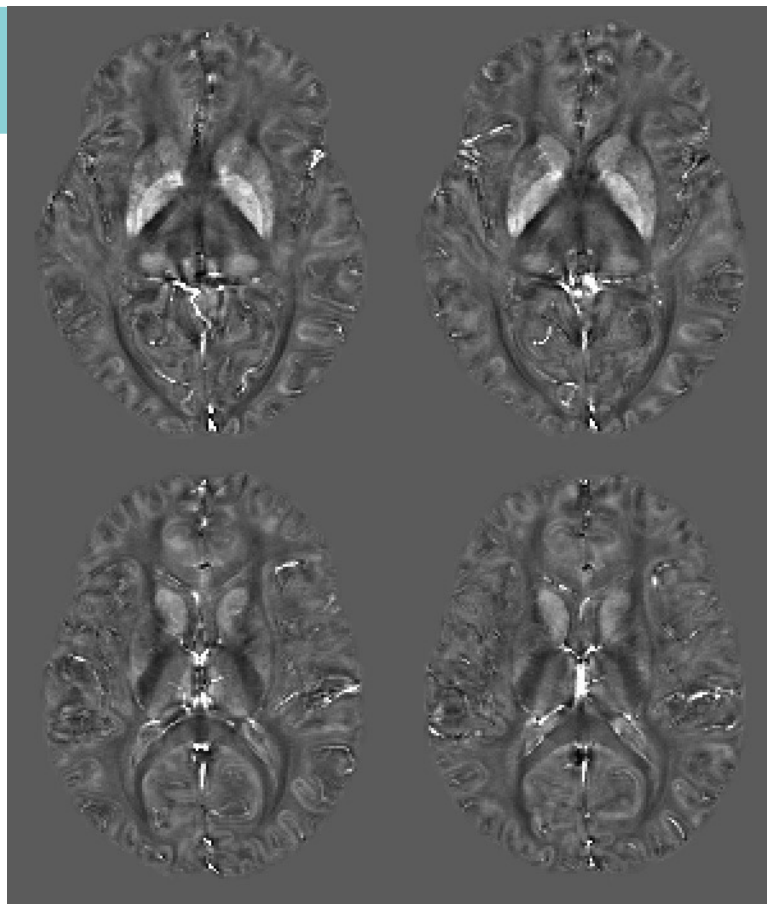
Phase MRI

Susceptibility MRI Contrast

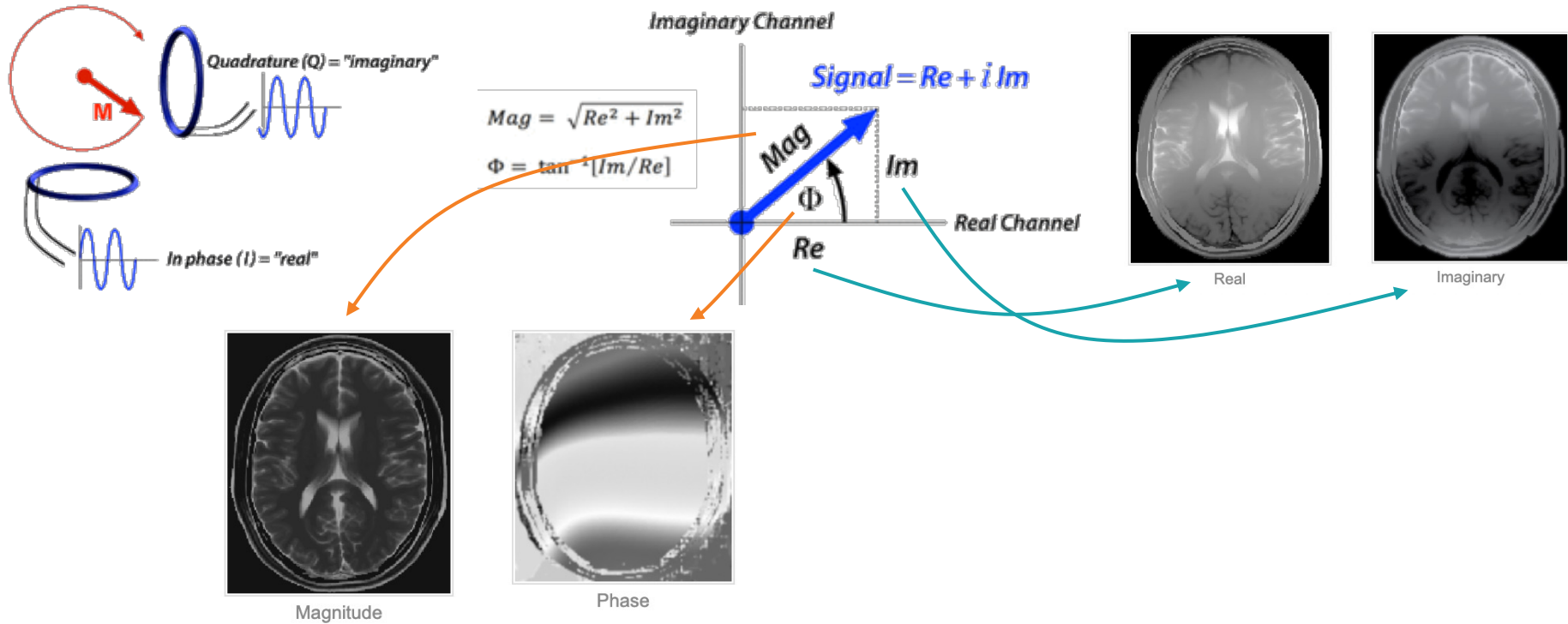
Susceptibility MRI Processing

Susceptibility MRI Applications

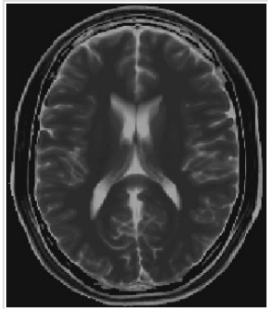
Conductivity MRI



Phase MRI

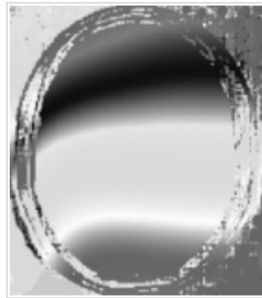


Phase MRI



Magnitude

Magnitude



Phase

Phase

Brain imaging

Structural imaging

- T1-weighted, T2-weighted, FLAIR

Function imaging

Diffusion and perfusion imaging

Susceptibility imaging

Cardiac imaging

Structural imaging

- Dark-blood and bright-blood sequences

Cardiac motion imaging

- Cine

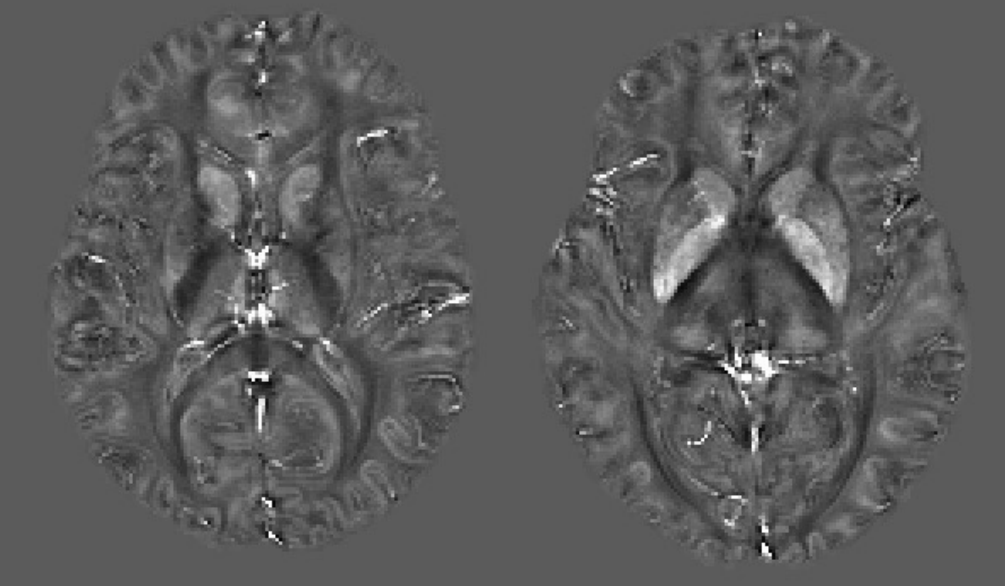
Perfusion imaging

Flow imaging

Phase MRI

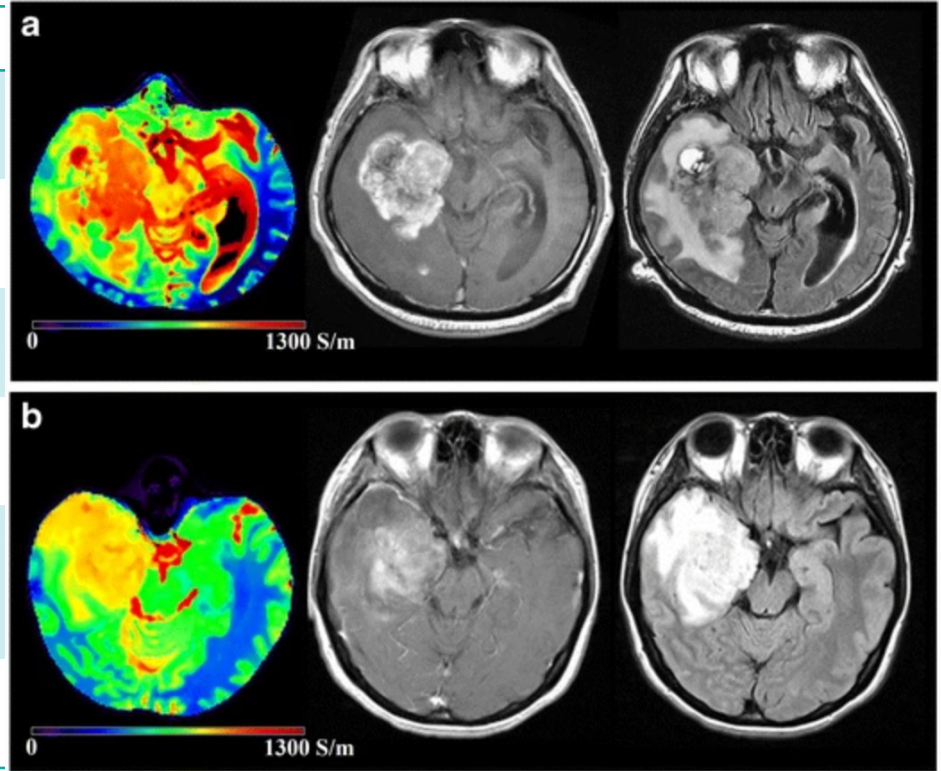
	Encoding	Data	Applications
Susceptibility imaging	None	Raw phase	Iron, calcium, myelin imaging
Conductivity imaging	None	Raw phase	Tumors, ischemic lesions
MR thermometry	None	Phase shift	MR-guided procedures
Flow imaging	Velocity-encoding bipolar gradient	Subtracted phase data from opposite encodings	Cardiac flow, CSF flow
Phase contrast angiography	Bipolar gradients applied along the x, y, and z axes sequentially	Subtracted phase data from opposite encodings and combined across three directions	Angiogram, venogram, aneurysm
Elastography	Motion-encoding gradients	Phase differences	Liver fibrosis, brain

Phase MRI

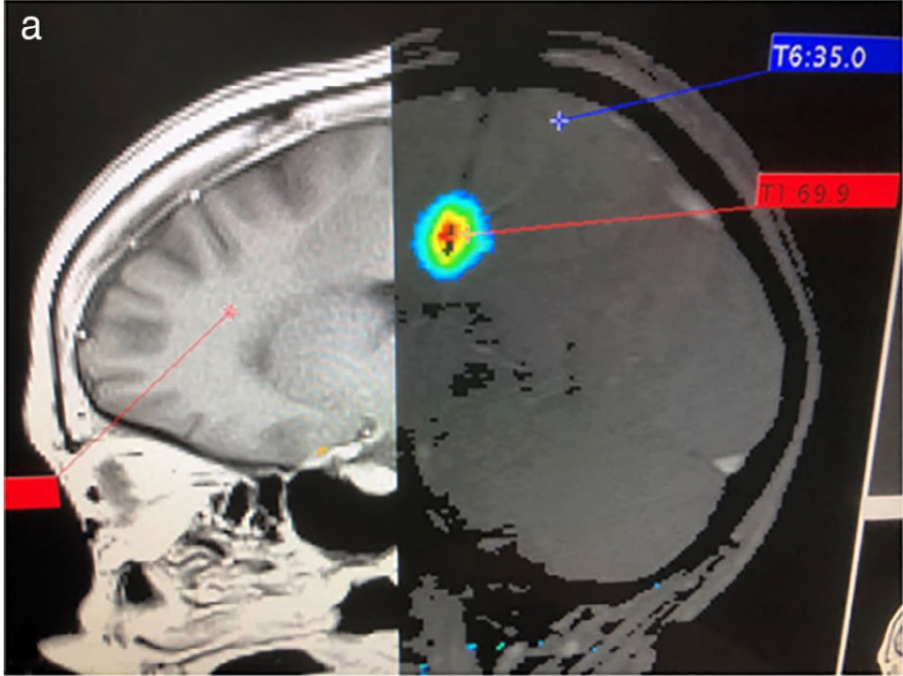
	Encoding	Data	Applications
Susceptibility imaging	None	Raw phase	Iron, calcium, myelin imaging
Conductivity imaging	None		
MR thermometry	None		
Flow imaging	Velocity-encoding bipolar gradient		
Phase contrast angiography	Bipolar gradients applied along the x and z axes sequentially		
Elastography	Motion-encoding gradients		

Phase MRI

	Encoding
Susceptibility imaging	None
Conductivity imaging	None
MR thermometry	None
Flow imaging	Velocity-encoding bipolar gradient
Phase contrast angiography	Bipolar gradients applied along the x, y, and z axes sequentially
Elastography	Motion-encoding gradients

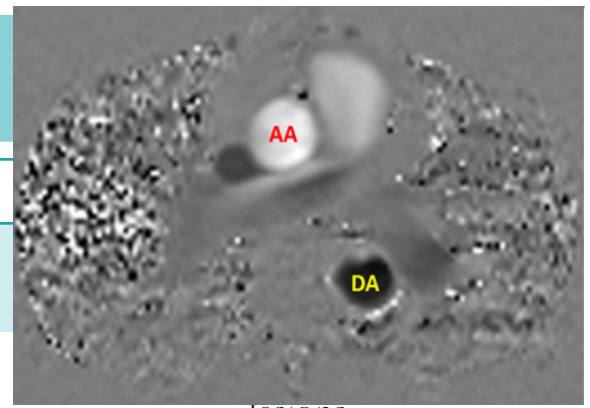


Phase MRI

	Encoding	Data	Applications
Susceptibility imaging	None		
Conductivity imaging	None		
MR thermometry	None		
Flow imaging	Velocity-encoding bipolar gradient		
Phase contrast angiography	Bipolar gradients applied along the x, y, and z axes sequentially		
Elastography	Motion-encoding gradients		

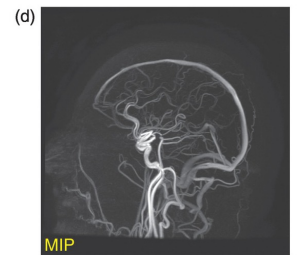
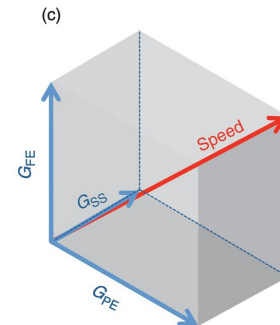
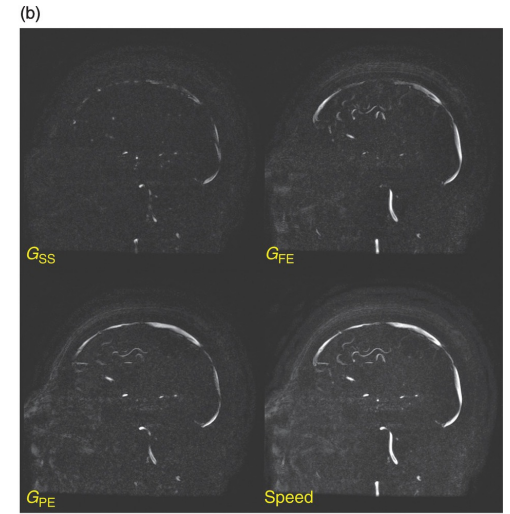
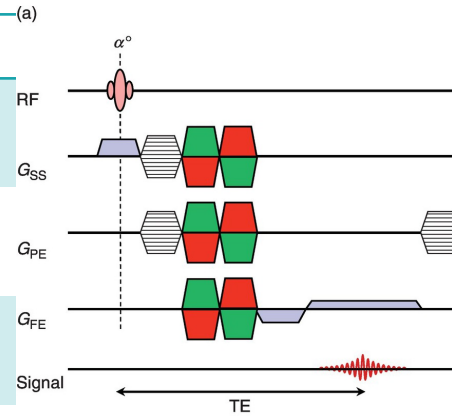
Phase MRI

	Encoding	Data
Susceptibility imaging	None	Raw phase
Conductivity imaging	None	Raw phase (B_1)
MR thermometry	None	Phase shift
Flow imaging	Velocity-encoding bipolar gradient	Subtracted phase data from opposite encodings
Phase contrast angiography	Bipolar gradients applied along the x, y, and z axes sequentially	Subtracted phase data from opposite encodings and combined across three directions
Elastography	Motion-encoding gradients	Phase differences



Phase MRI

	Encoding
Susceptibility imaging	None
Conductivity imaging	None
MR thermometry	None
Flow imaging	Velocity-encoding bipolar gradient
Phase contrast angiography	Bipolar gradients applied along the x, y, and z axes sequentially
Elastography	Motion-encoding gradients



Phase MRI

Susceptibility imaging

Conductivity imaging

MR thermometry

Flow imaging

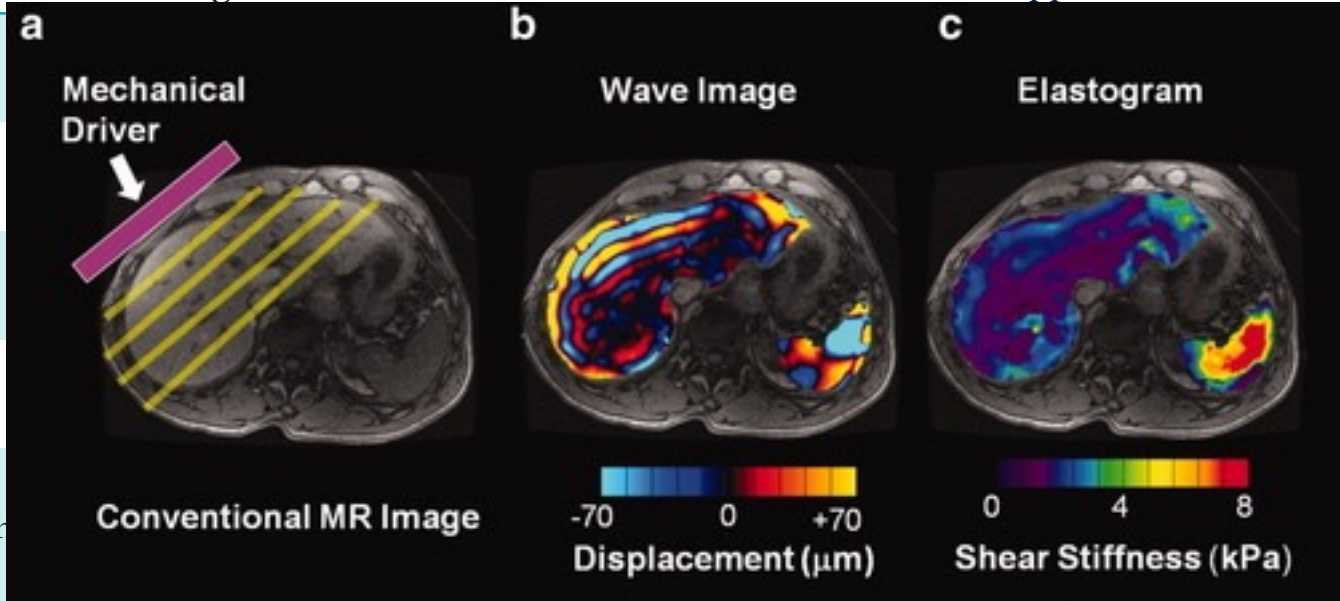
Phase contrast angiography

Elastography

Encoding

Data

Applications



Motion-encoding
gradients

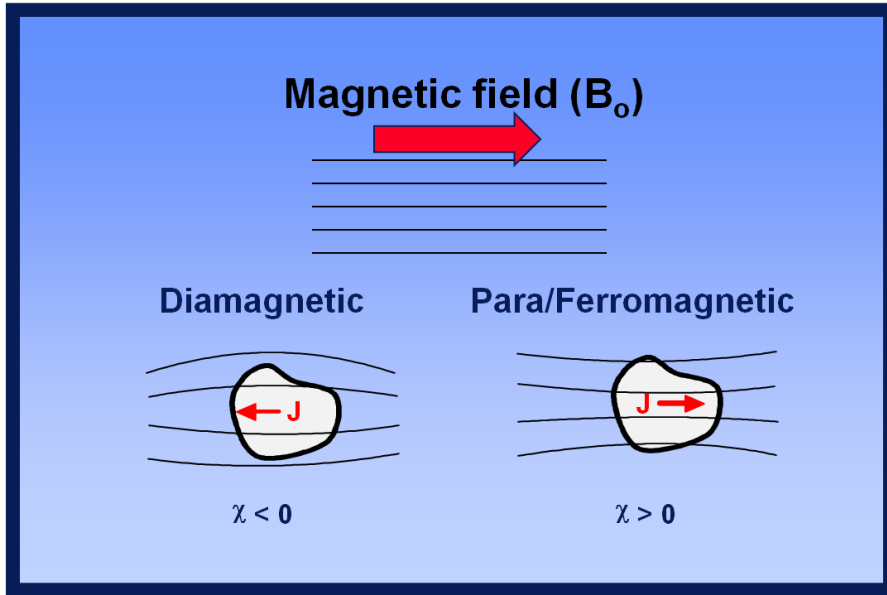
Phase differences

Liver fibrosis, brain

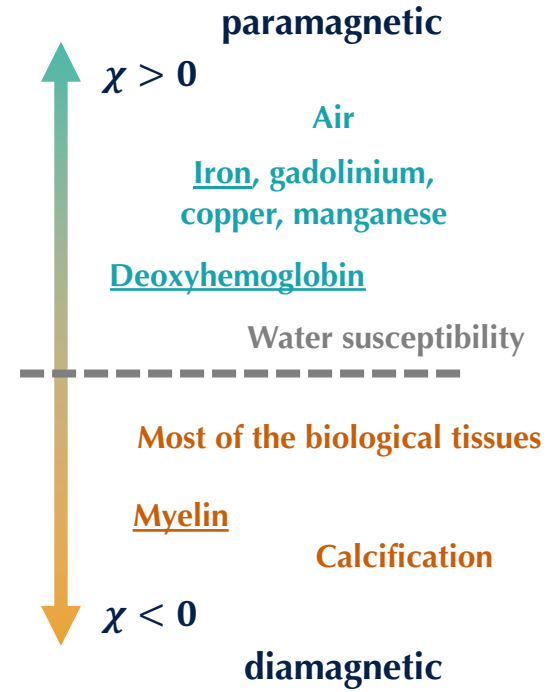
Phase MRI

	Encoding	Data	Applications
Susceptibility imaging	None	Raw phase	Iron, calcium, myelin imaging
Conductivity imaging	None	Raw phase (B_1)	Tumors, ischemic lesions
MR thermometry	None	Phase shift	MR-guided procedures
Flow imaging	Velocity-encoding bipolar gradient	Subtracted phase data from opposite encodings	Cardiac flow, CSF flow
Phase contrast angiography	Bipolar gradients applied along the x, y, and z axes sequentially	Subtracted phase data from opposite encodings and combined across three directions	Angiogram, venogram, aneurysm
Elastography	Motion-encoding gradients	Phase differences	Liver fibrosis, brain

Susceptibility MRI – source of contrast



$$J = \chi B_0$$

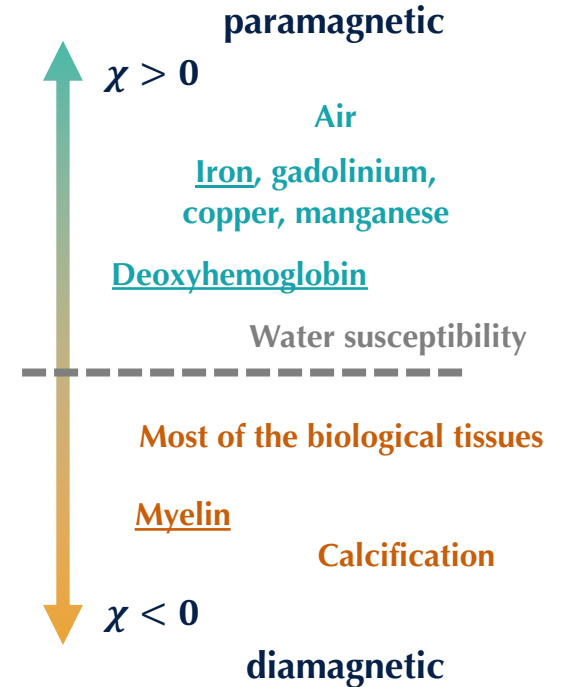
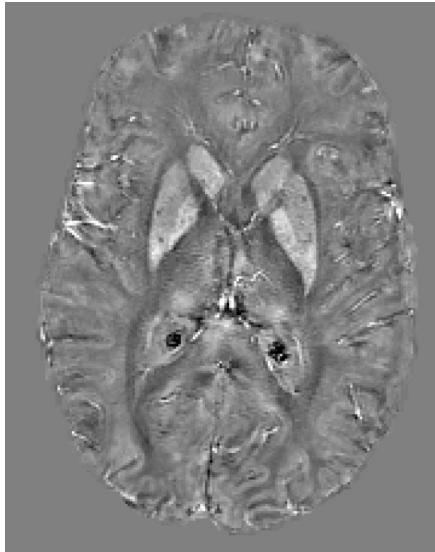


Susceptibility MRI – source of contrast

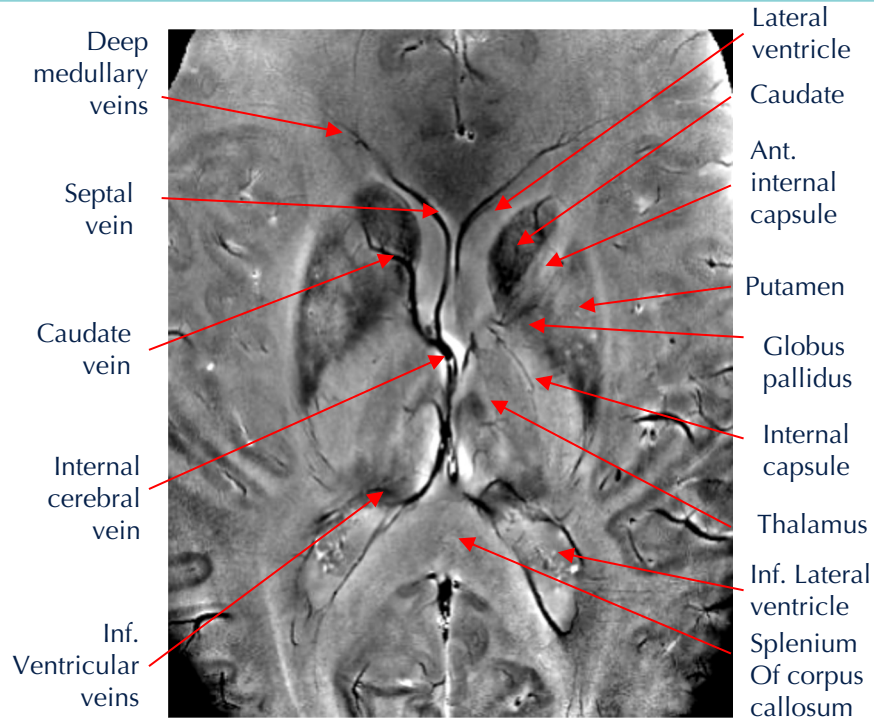
Susceptibility-weighted imaging



Quantitative susceptibility mapping



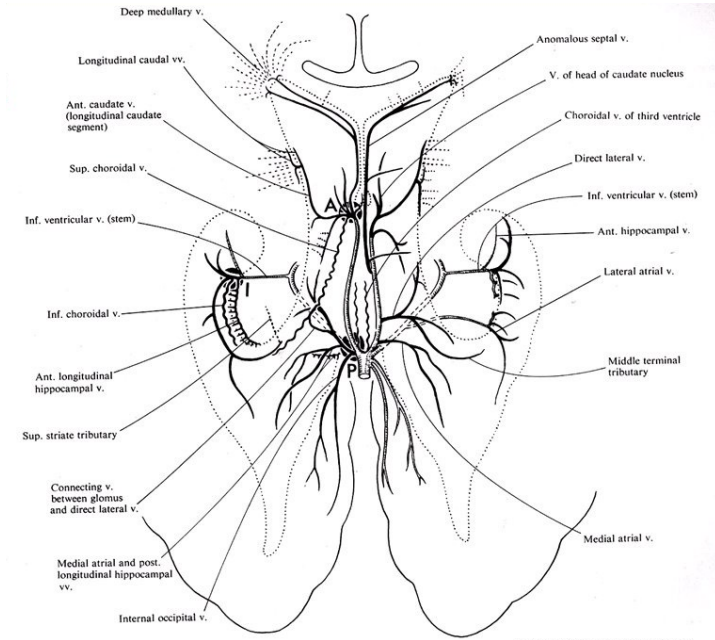
Susceptibility MRI – Deoxyhemoglobin



VEINS

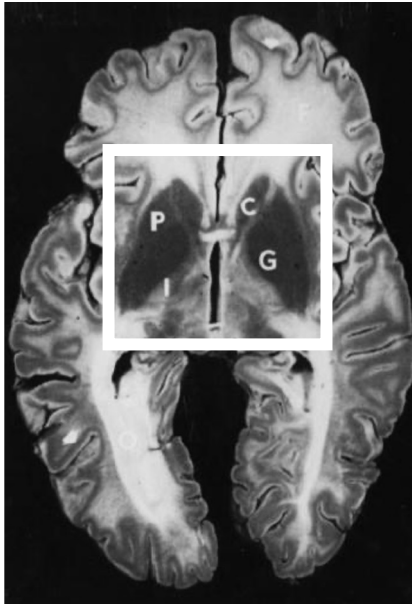
GRE Phase Image

STRUCTURES

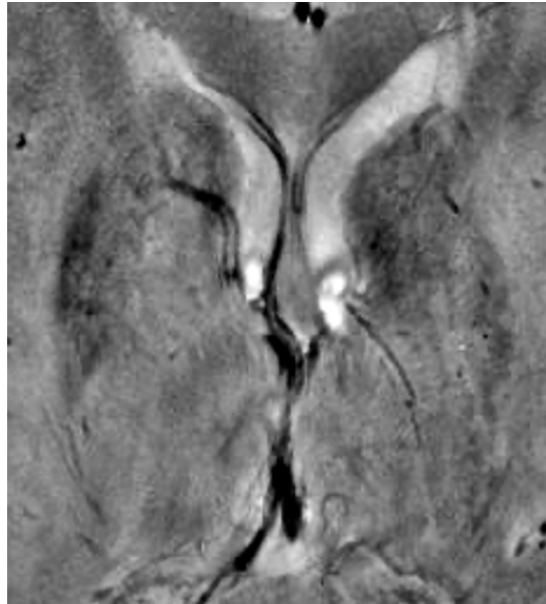


from G Salamon, Y.P. Huang Radiologic Anatomy of the brain, Springer verlag 1976

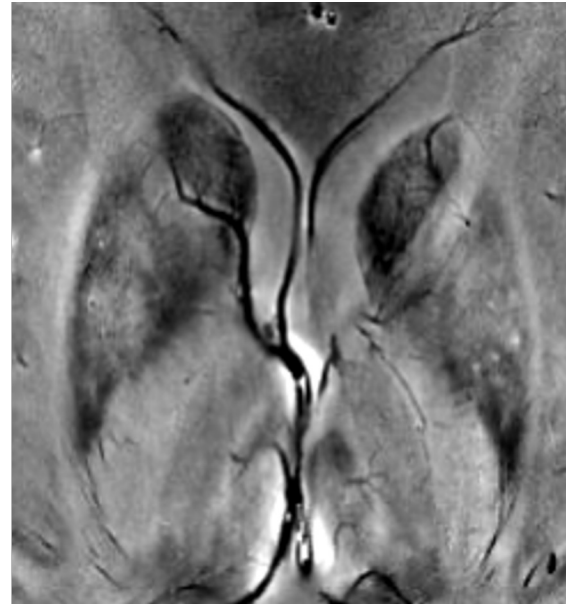
Susceptibility MRI – Iron



Iron Perl's Stain

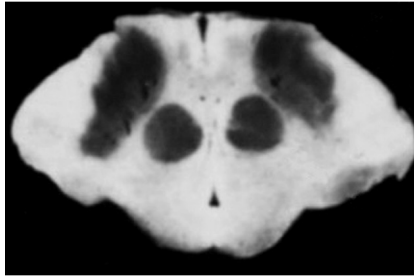


GRE Magnitude Image

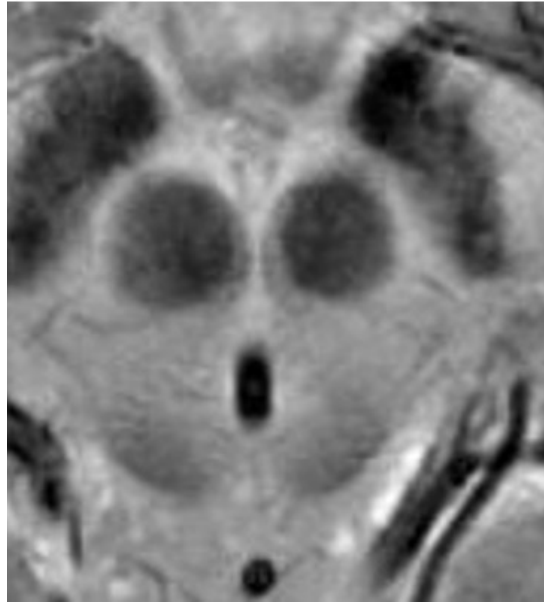


GRE Phase Image

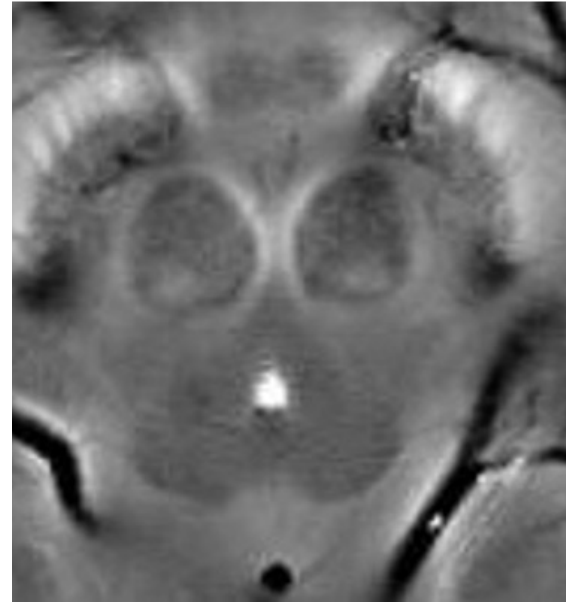
Susceptibility MRI – Iron



Iron Perl's Stain

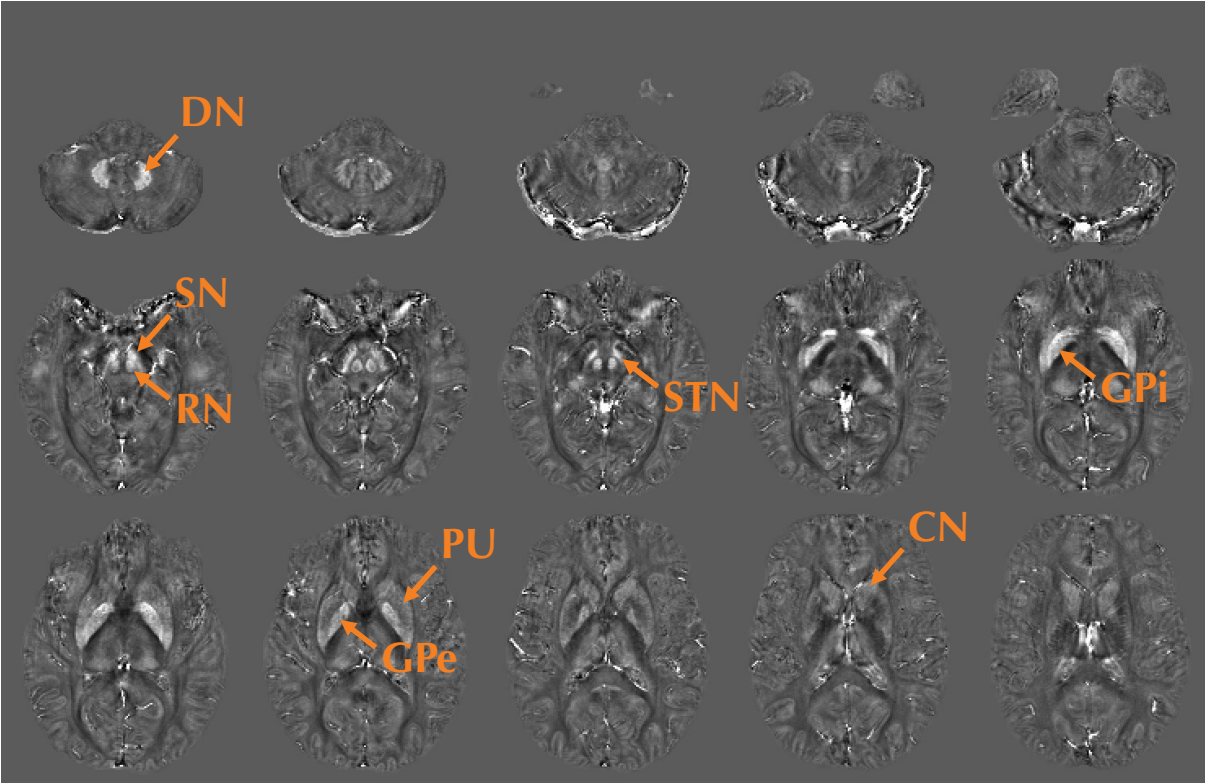


GRE Magnitude Image

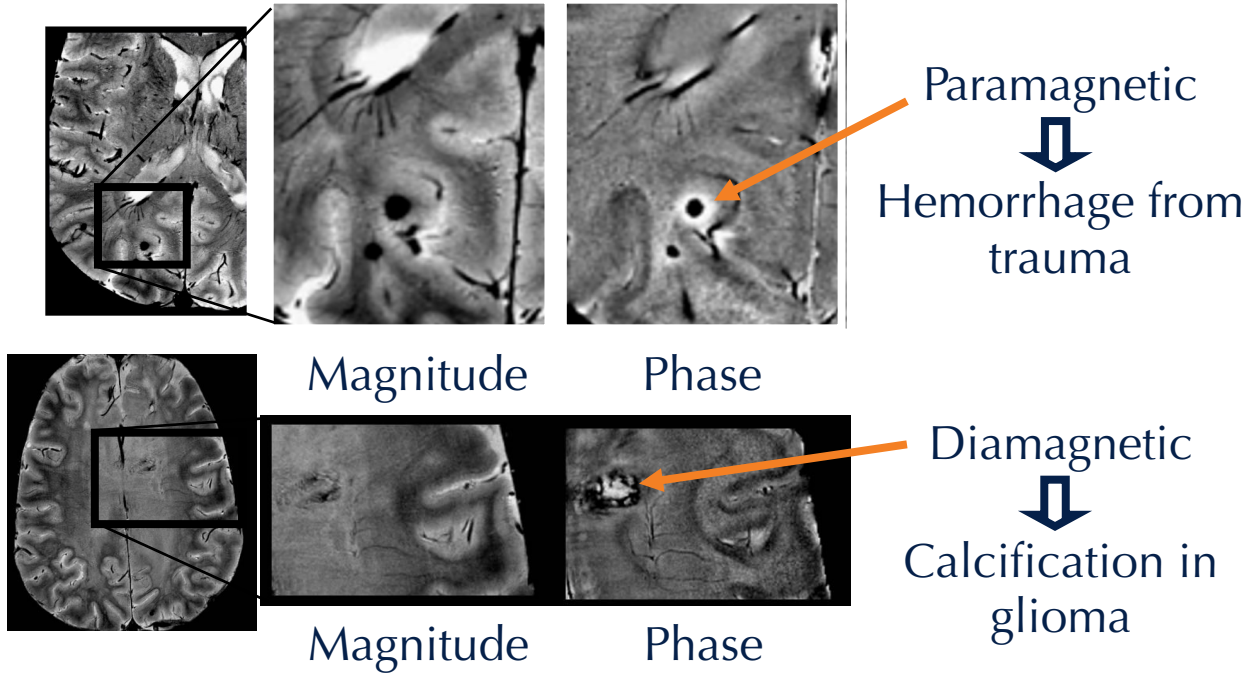


GRE Phase Image

Susceptibility MRI – Iron

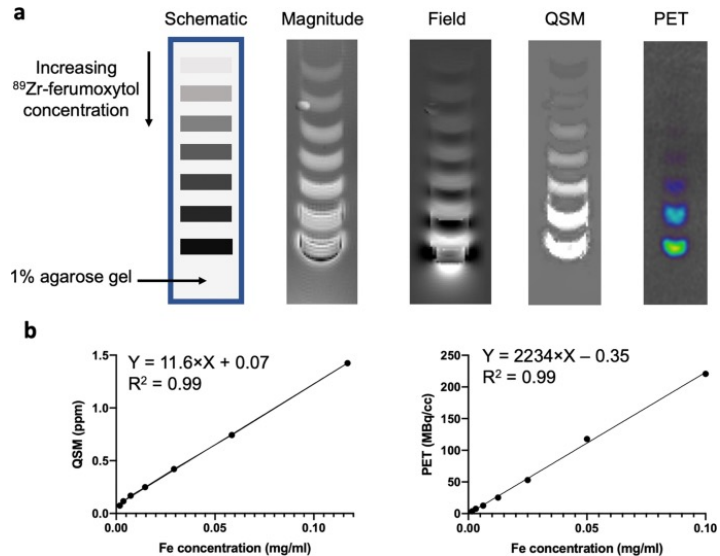


Susceptibility MRI – Calcification

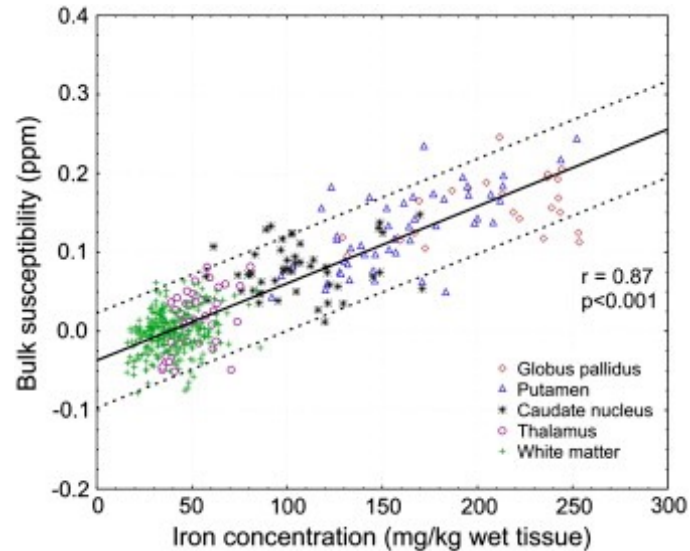


Susceptibility MRI – Iron

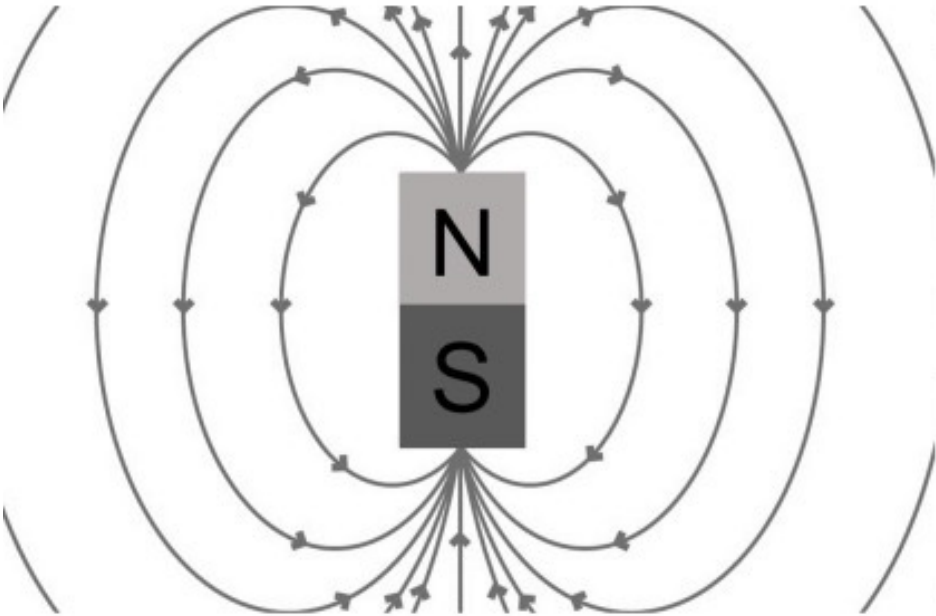
Phantom validation



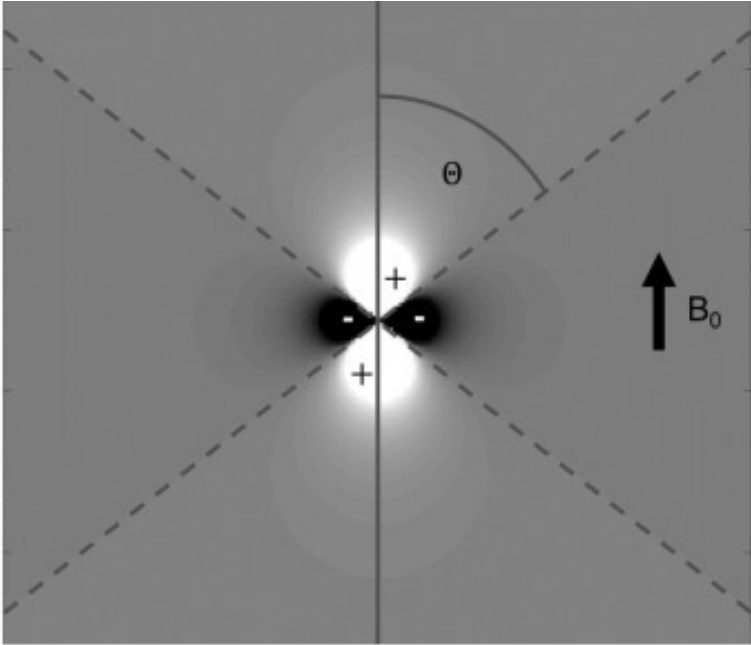
Tissue validation



Susceptibility MRI – Signal model



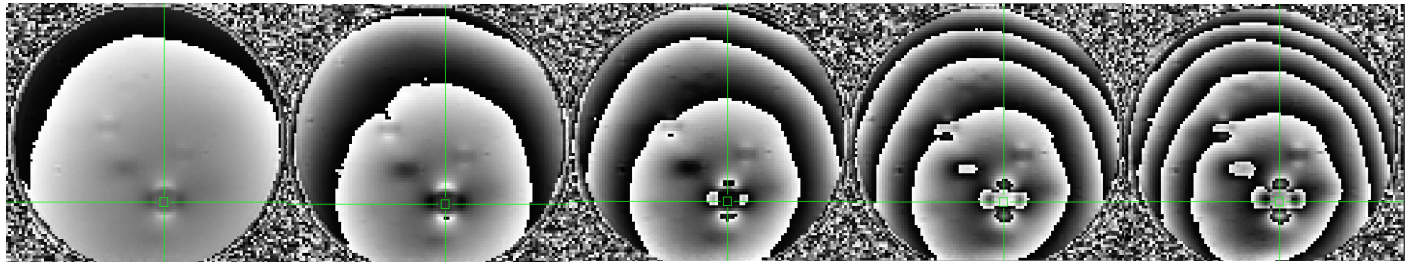
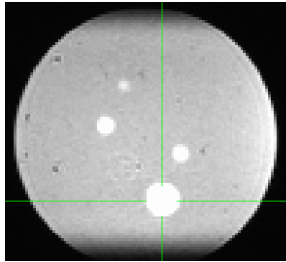
a)



b)

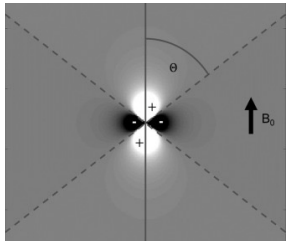
Susceptibility MRI – Signal model

Ferumoxytol phantom

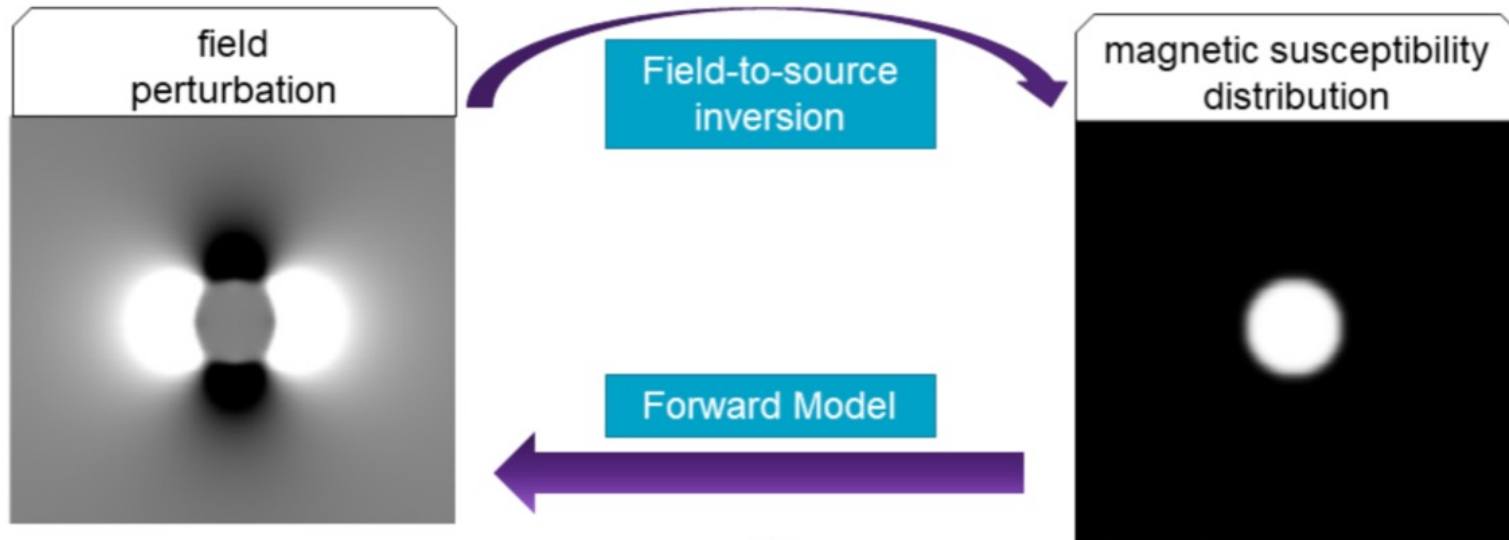


5.84 ms

40.56 ms



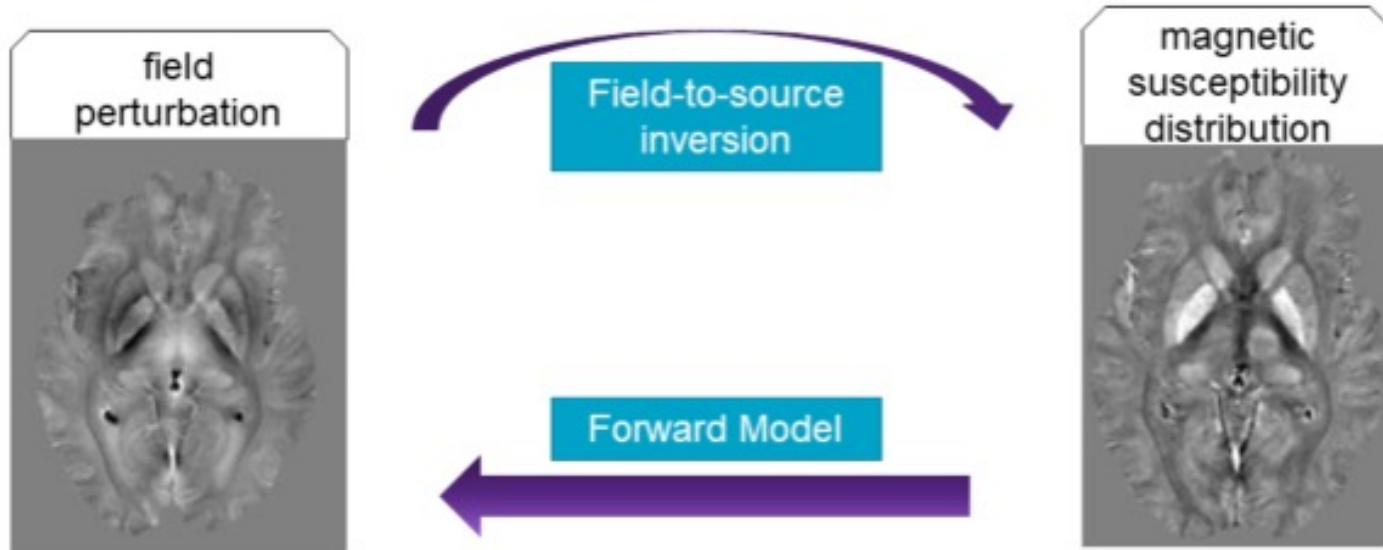
Susceptibility MRI – Signal model



$$\Delta B_{\text{int}}(\vec{r}) = B_0 \cdot \int_{-\infty}^{\infty} \tilde{\chi}(\vec{r}') \cdot d_z(\vec{r} - \vec{r}') d^3 r'$$

Review: Deistung et al. NMR Biomed 2017; Schweser et al. Z Med Phys 2016

Susceptibility MRI – Signal model

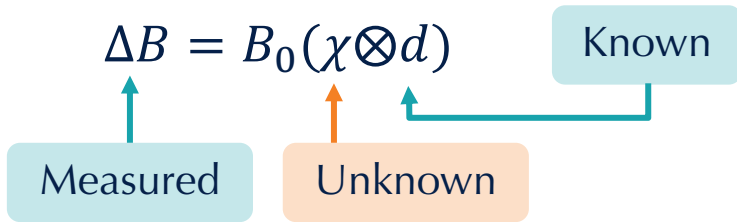


$$\Delta B_{\text{int}}(\vec{r}) = B_0 \cdot \int_{-\infty}^{\infty} \tilde{\chi}(\vec{r}') \cdot d_z(\vec{r} - \vec{r}') d^3 r'$$

Review: Deistung et al. NMR Biomed 2017; Schweser et al. Z Med Phys 2016

Susceptibility MRI – Signal model

$$\Delta B(\vec{r}) = B_0 \int_{-\infty}^{\infty} \chi(\vec{r}') d(\vec{r} - \vec{r}') d^3 \vec{r}'$$



FT

$$\Delta B(\vec{k}) = B_0[\chi(\vec{k})d(\vec{k})]$$

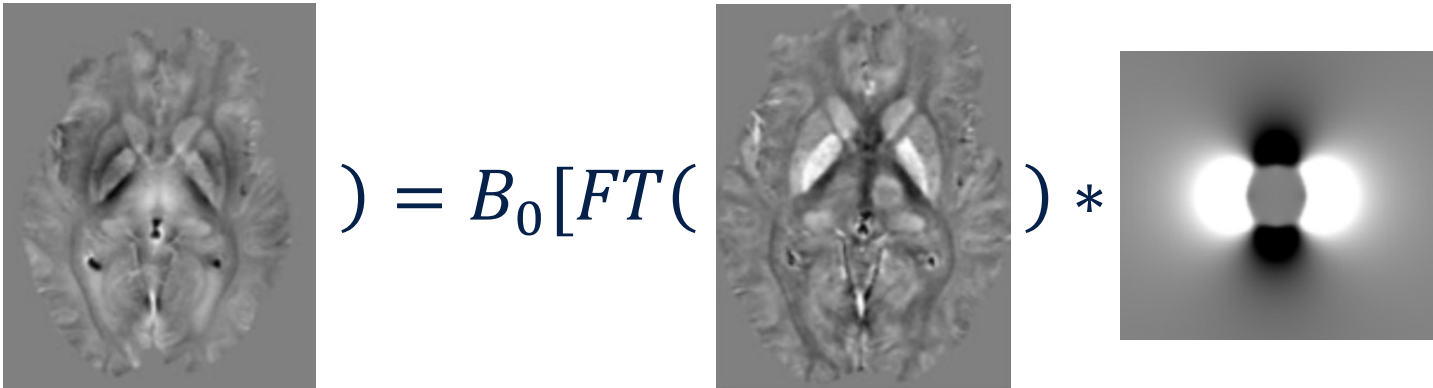
$$d(\vec{r}) = \frac{1}{4\pi} \frac{3 \cos^2(\theta) - 1}{|\vec{r}|^3}$$

$$d(\vec{k}) = \frac{1}{3} - \frac{k_z^2}{|\vec{k}|^2}$$

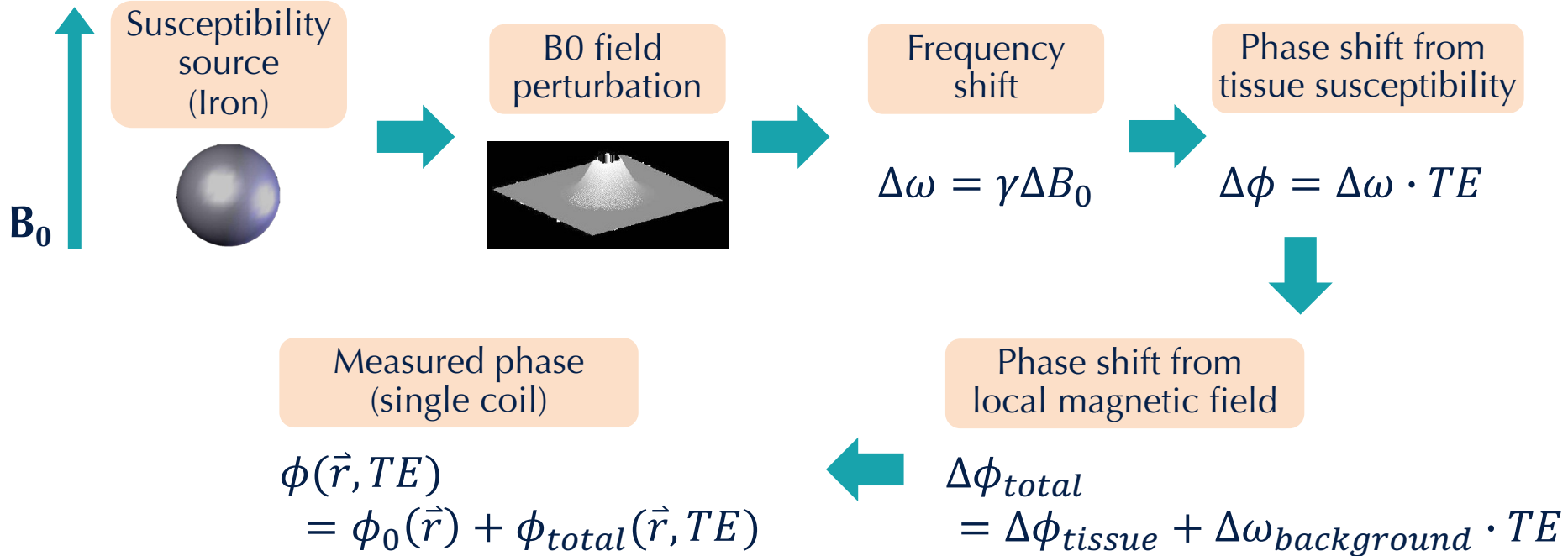
Susceptibility MRI – Signal model

$$\Delta B(\vec{k}) = B_0[\chi(\vec{k})d(\vec{k})]$$

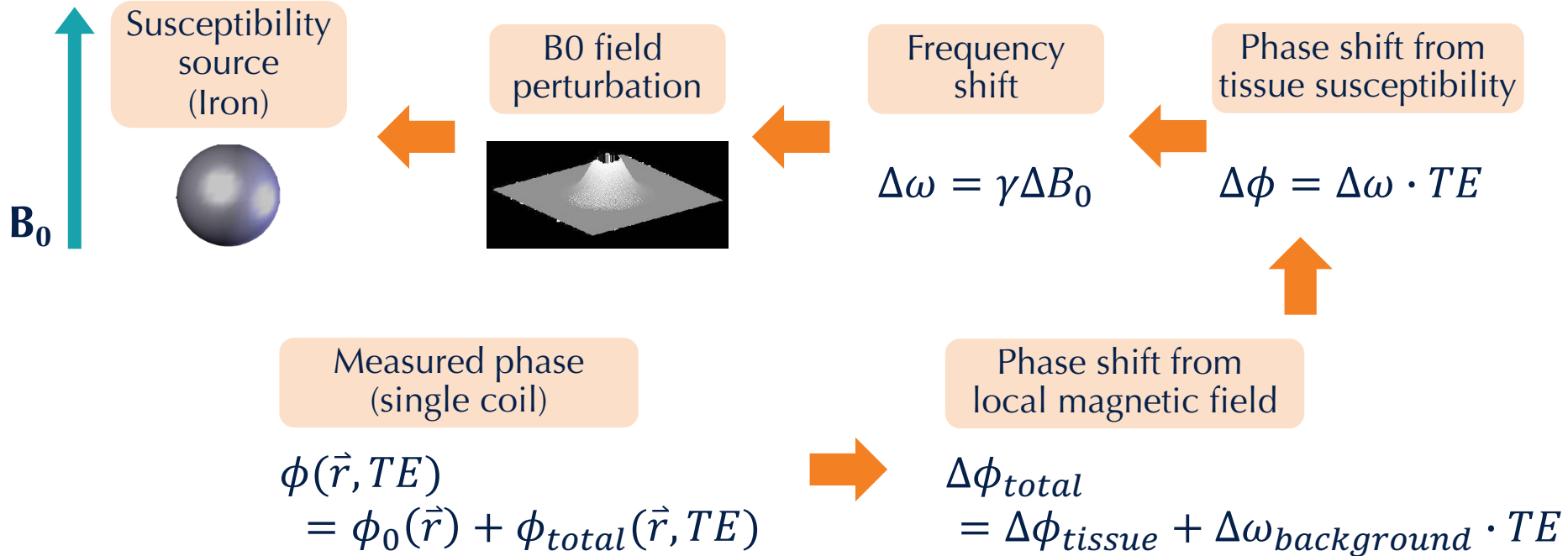
$$d(\vec{k}) = \frac{1}{3} - \frac{k_z^2}{|\vec{k}|^2}$$

$$FT(\text{Image 1}) = B_0[FT(\text{Image 2}) * \text{Image 3}]$$


Susceptibility MRI – Signal model



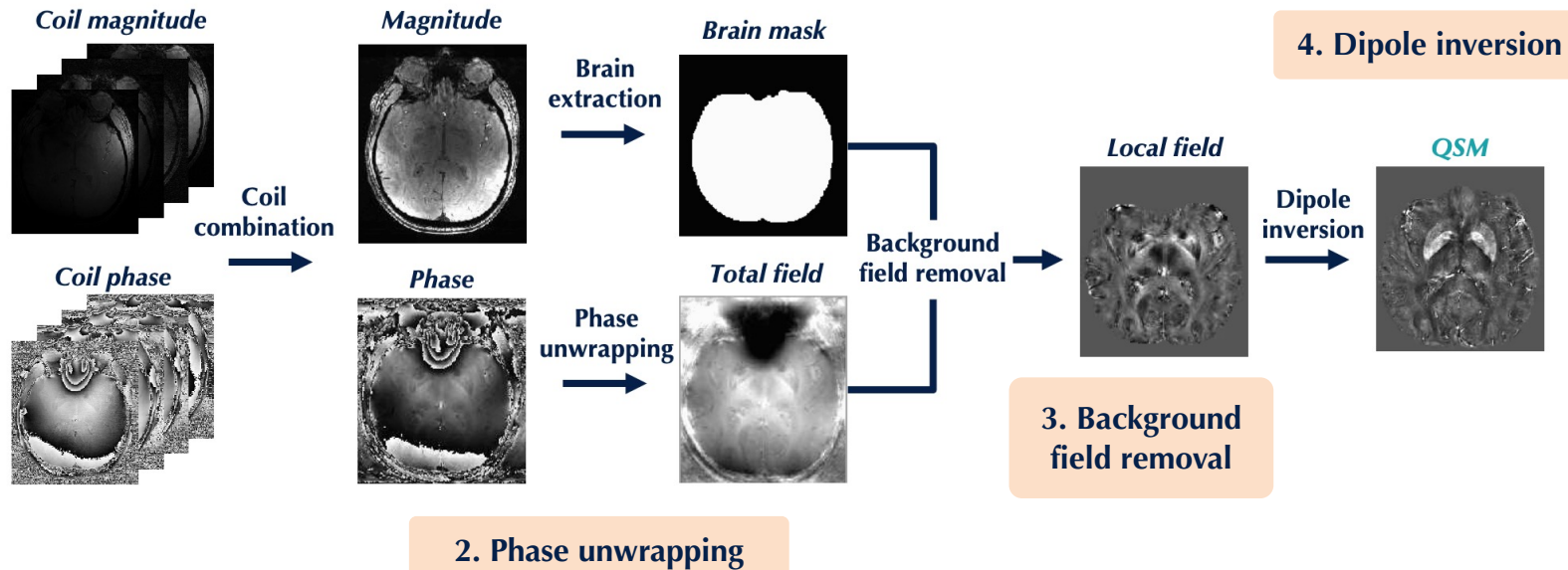
Susceptibility MRI – Processing



QSM - Processing

1. Image acquisition

T_2^* -weighted sequence



QSM - Processing

1. Image acquisition

T_2^* -weighted sequence

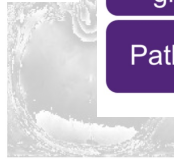
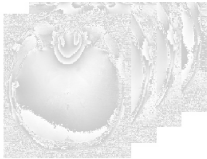
Coil magnitude

Magnitude

Phase combination approaches

- 1 echo, No reference scan
 - Scalar phase matching [1]
 - Adaptive combine [2]
 - Virtual Reference Coil [3]
- 1 echo, Reference scan
 - Roemer/SENSE [4]
 - COMPOSER [5]
- Multiple echoes
 - SVD [6]
 - Solve for ΔB_0 via phase difference [7]
 - Solve for φ_0^c : ASPIRE [8]

[1] Hammond et al. NI 2008
 [2] Walsh et al. MRM 2000
 [3] Parker et al. MRM 2004
 [4] Roemer et al. NI 1990
 [5] Robinson et al. MRM 2017
 [6] Khabipova et al. NI 2015
 [7] Barnetson et al. MRM 1994
 [8] Eckstein et al. MRM 2018
 Review: Robinson et al. NMR Biomed 2017



Background field correction methods & assumptions

- no sources close to boundaries
 - SHARP (Schweser et al. NI 2011)
 - V-SHARP (Li et al. NI 2011)
- no harmonic internal and boundary fields
 - LBV (Zhou et al. NMR Biomed 2014)
- no implicit boundary assumption
 - RESHARP (Sun et al. MRM 2014)
 - SHARQnet (Bollmann et al. Z Med Phys 2018)

Unwrapping techniques

- Laplacian
 - differentiable operator applied to the unwrapped phase can produce the same result on the wrapped phase \rightarrow Laplacian (Schofield and Zhu, Opt Lett. 2003)
 - + fast & robust
 - - introduces background phase
- Region-growing
 - identify discontinuities between regions
 - PRELUDE (Jenkinson MRM 2003) can take a while to compute for highly wrapped data
 - SEQUE (Kersa et al. TMI 2019) similar accuracy to PRELUDE, but faster
- Path Based
 - 3D voxel-by-voxel unwrapping guided by the quality of voxel connections
 - BEST PATH (Abdul-Rahman et al. AO 2007)
 - ROMEO (Dymarska et al. MRM 2021)

Review: Robinson et al. NMR Biomed 2017

2. Phase unwrapping

4. Dipole inversion

Dipole inversion methods & assumptions

- multiple orientations
 - COSMOS (Liu et al. MRM 2009)
 - STI (Liu MRM 2010)
 - analytical solutions, but not practical
- inverse filtering
 - TND (Shrout et al. MRM 2009)
 - fast, but need parameter tweaking
- iterative methods
 - LSQR (Li et al. NI 2015)
 - MEDI (Liu et al. MRM 2013)
 - slow, need parameter tweaking
- agnostic deep learning
 - GSMNet (Yoon et al. NI 2018)
 - DeepQSM (Bollmann et al. NI 2019)
 - fast, but fragile
- hybrid methods
 - FINE (Zhang et al. NI 2020)
 - Variational Networks (Liu et al. arXiv 2020)
 - Deep learning priors + data consistency constraints

Reviews: Schweser et al. NMR Biomed 2017; Jung et al. NMR Biomed 2020

3. Background field removal

Special issue review article

Received: 11 November 2015,

Revised: 14 June 2016,

Accepted: 18 July 2016,

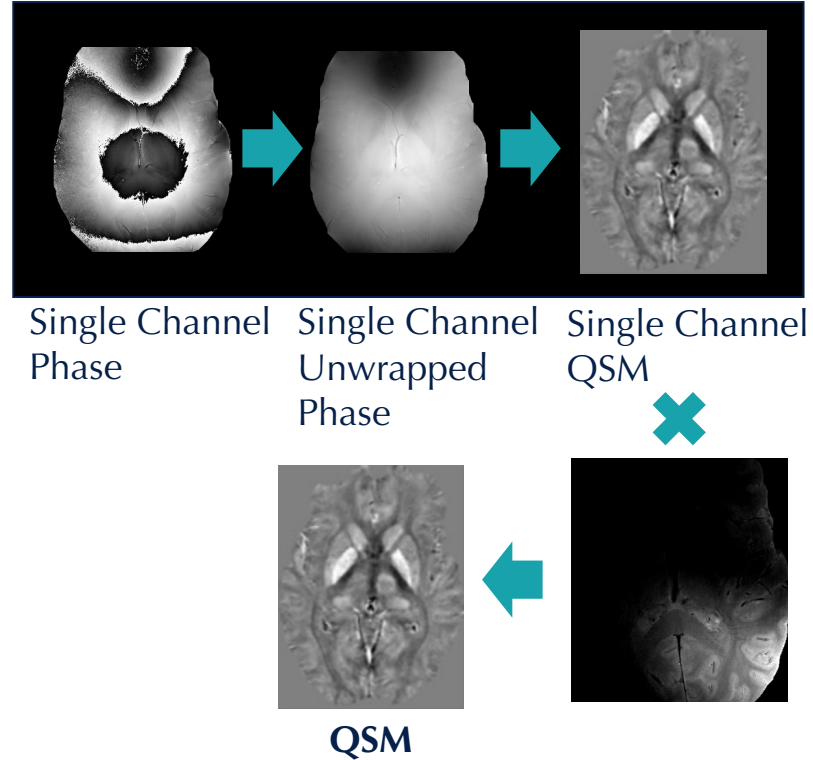
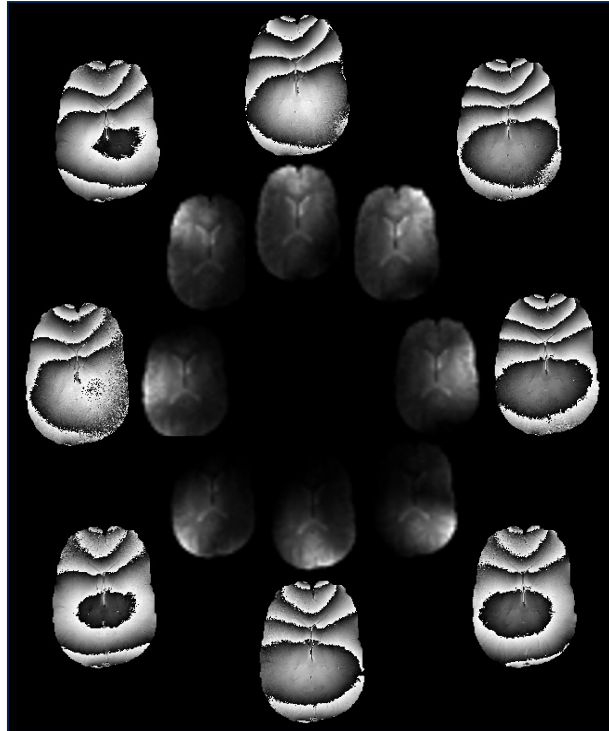
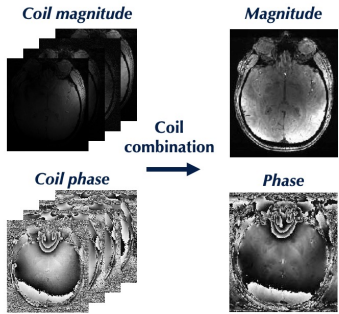
Published online in Wiley Online Library: 13 September 2016

(wileyonlinelibrary.com) DOI: 10.1002/nbm.3601

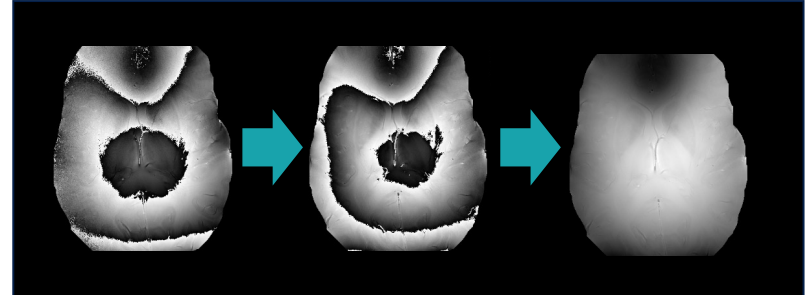
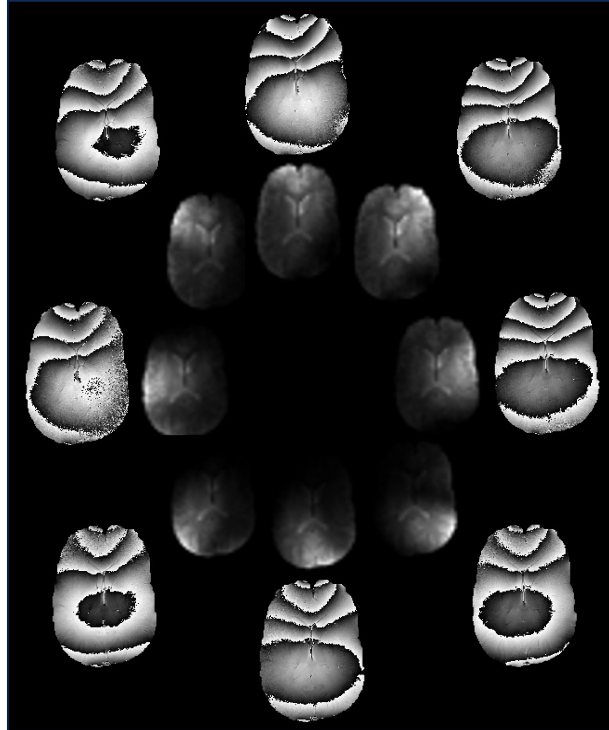
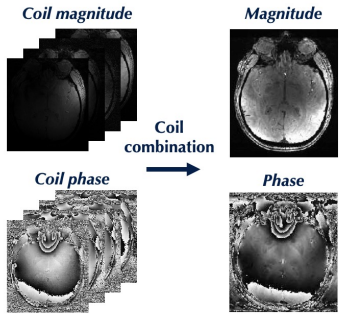
An illustrated comparison of processing methods for MR phase imaging and QSM: combining array coil signals and phase unwrapping

Simon Daniel Robinson^{a*}, Kristian Bredies^b, Diana Khabipova^{c,d},
Barbara Dymerska^a, José P. Marques^{c,d} and Ferdinand Schweser^{e,f}

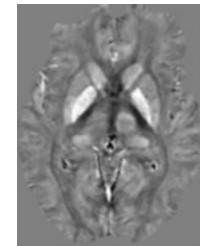
QSM - Coil Combination



QSM - Coil Combination

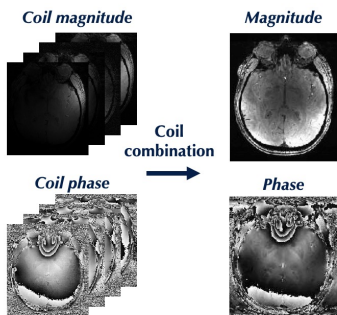


Single Channel Phase Multi Channel Phase Unwrapped Phase



QSM

QSM - Coil Combination



Measured phase
(single coil)

$$\phi(\vec{r}, TE) = \phi_0(\vec{r}) + \phi_{total}(\vec{r}, TE)$$

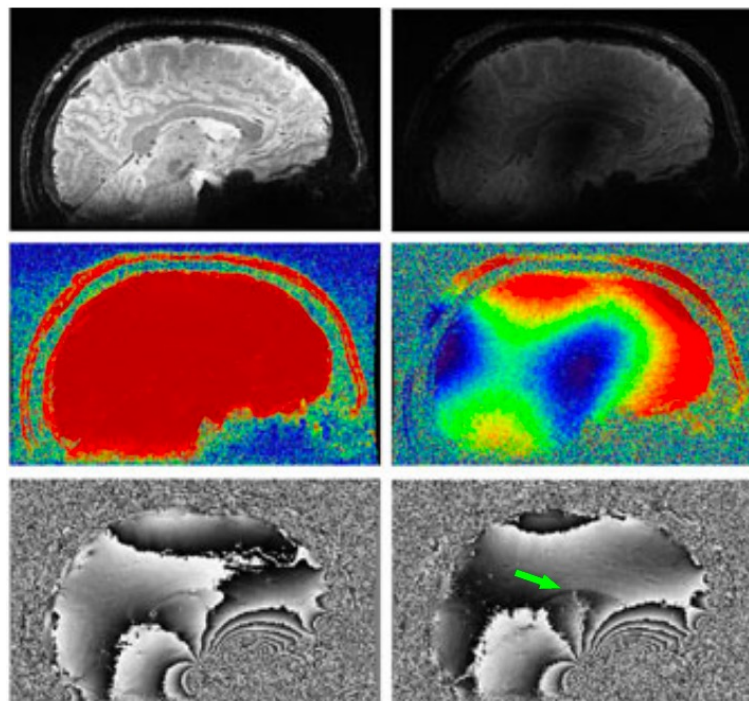


Transceive phase

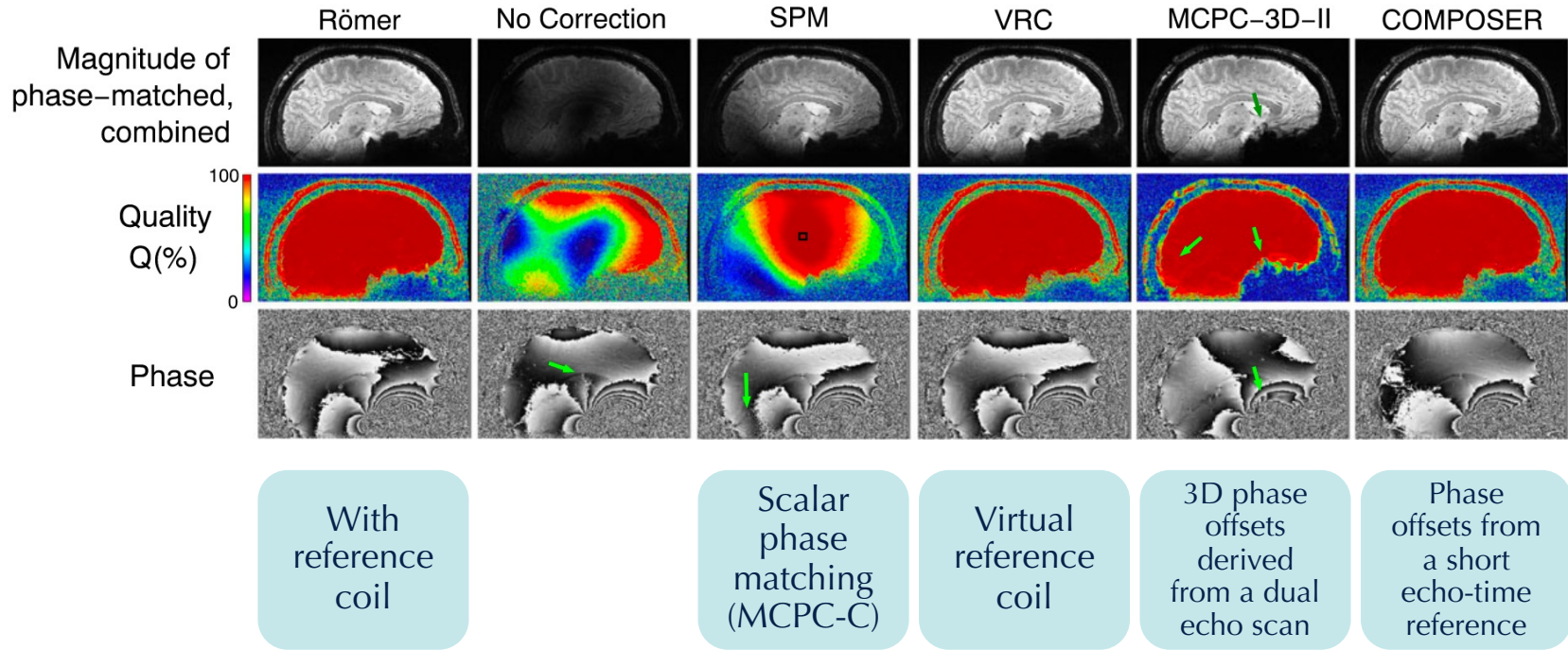
spatially varying phase offsets exist between receive coils

Römer

No Correction



QSM - Coil Combination



$$\varphi_j^0(\vec{r}) = \frac{\varphi_j(\vec{r}, TE_2)TE_1 - \varphi_j(\vec{r}, TE_1)TE_2}{TE_1 - TE_2}$$

QSM - MPCP-3D

Steps:

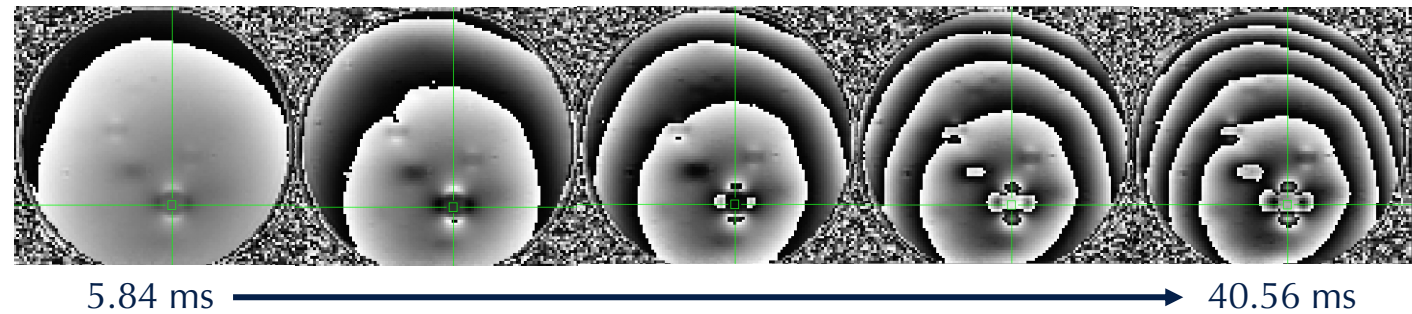
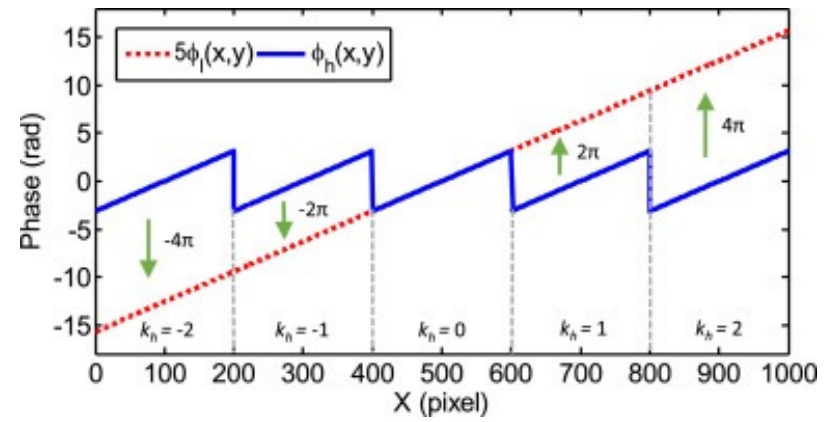
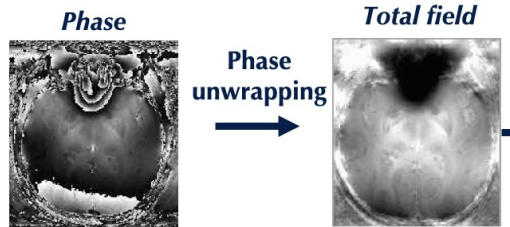
- unwrap each echo phase
- create 3D phase offset map for each coil using each unwrapped echo
- smooth with 5x5 median filter
- subtract 3D phase offset map from phase image of each channel
- weighted mean

$$\varphi_j^0(\vec{r}) = \frac{\varphi_j(\vec{r}, TE_2)TE_1 - \varphi_j(\vec{r}, TE_1)TE_2}{TE_1 - TE_2}.$$

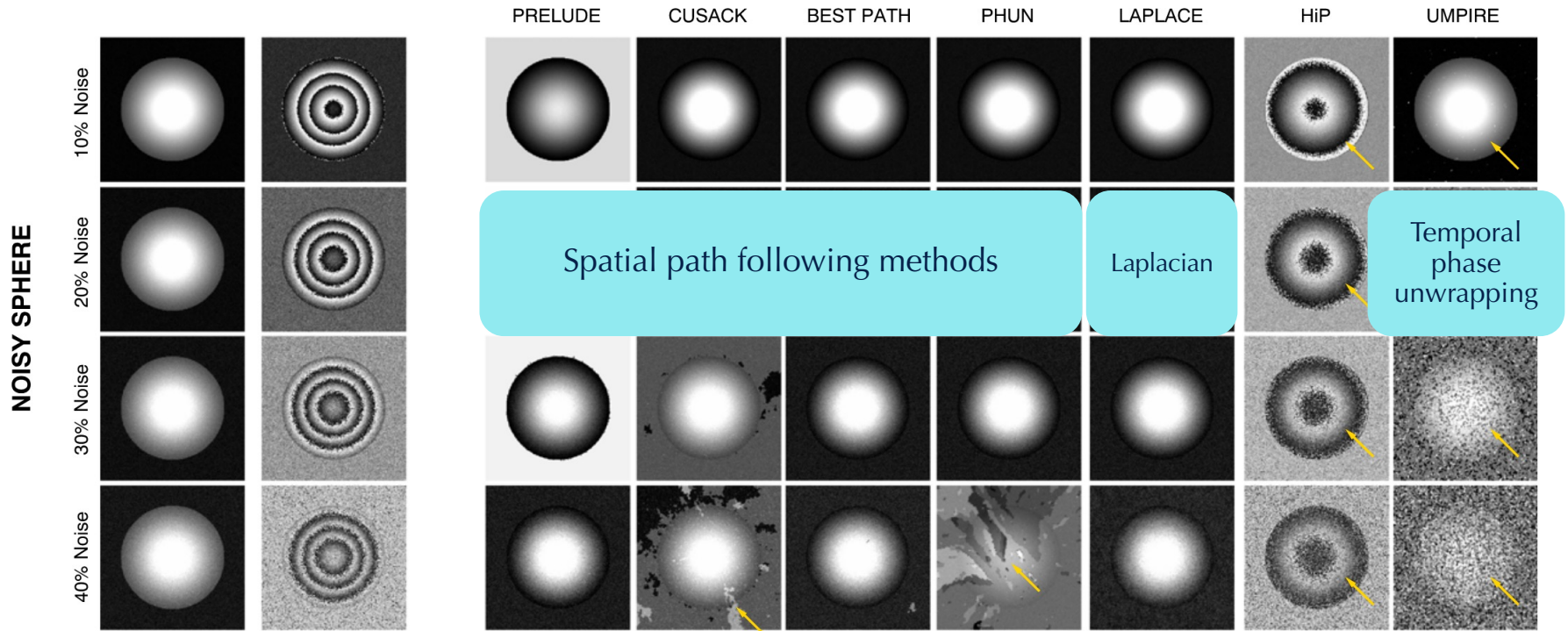
Advantages:

- works where there is no signal overlap between receivers
- no need for reference coil
- also works using a separate low-resolution scan

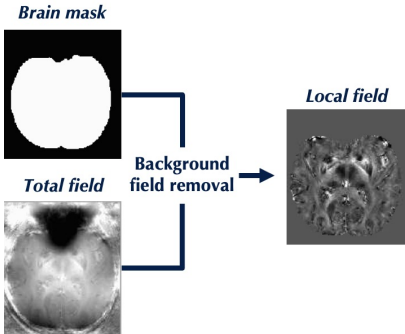
QSM - Phase unwrapping



QSM - Phase unwrapping



QSM - Background field removal



Journal of Magnetic Resonance 148, 442–448 (2001)
doi:10.1006/jmre.2000.2267, available online at <http://www.idealibrary.com> on IDEAL®

High-Precision Mapping of the Magnetic Field Utilizing the Harmonic Function Mean Value Property

Lin Li and John S. Leigh

Department of Biochemistry and Molecular Biophysics, and Metabolic Magnetic Resonance Research & Computing Center, Department of Radiology, University of Pennsylvania, Philadelphia, Pennsylvania 19104

Received June 15, 2000; revised November 20, 2000

The spatial distributions of the static magnetic field components and MR phase maps in space with homogeneous magnetic susceptibility are shown to be harmonic functions satisfying Laplace's equation. A mean value property is derived and experimentally confirmed on phase maps: the mean value on a spherical surface in space is equal to the value at the center of the sphere. Based on this property, a method is implemented for significantly improving the precision of MR phase or field mapping. Three-dimensional mappings of the static magnetic field with a precision of $10^{-11} \sim 10^{-12}$ T are obtained in phantoms by a 1.5-T clinical MR scanner, with about three-orders-of-magnitude precision improvement over the conventional phase mapping technique. *In vivo* application of the method is also demonstrated on human leg phase maps. © 2001 Academic Press

Key Words: field mapping; harmonic function; mean value property; phase; SMV.

aging, we generate field maps with high precision up to $10^{-11} \sim 10^{-12}$ T. Such a measurement precision is comparable with that of a superconducting quantum interference device (SQUID) for the magnetic field measurement (17). Feasibility with *in vivo* applications is also demonstrated.

THEORY

In free space or regions without susceptibility heterogeneity and no macroscopic currents, all the components of the static magnetic field \mathbf{H} satisfy Laplace's equation, i.e., $\nabla^2 \mathbf{H}_i = 0$, $i = x, y, z$, or $\nabla^2 \mathbf{H} = 0$, which can be easily derived by setting the temporal derivative of the magnetic field in the electromagnetic wave equation (18) to zero. Therefore, local magnetic induction (4, 19) experienced by a nucleus, $(1 + \chi/3)H$, also satisfies Laplace's equation. Since the spatial

VSHARP

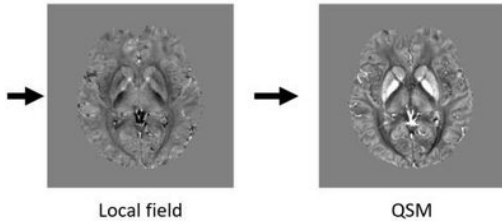
RESHARP

HARPERELLA

PDF

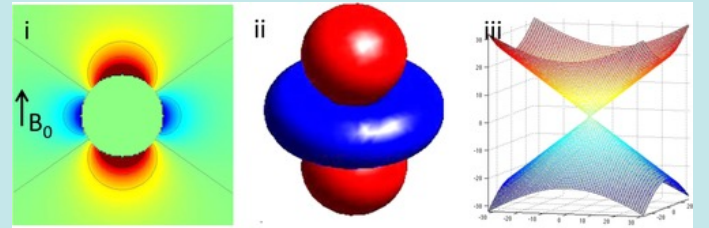
QSM - Dipole Inversion

Dipole inversion



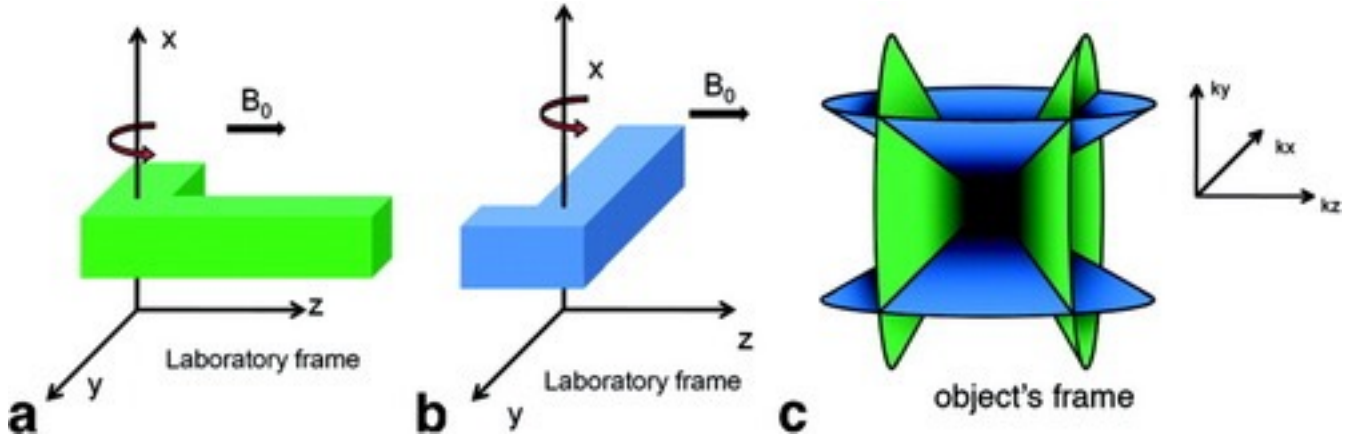
$$FT(\text{QSM}) = B_0 [FT(\text{Local field}) * \text{Dipole kernel}]$$

ill-posed inversion problem
 Noise amplification near the
 zero cone surfaces



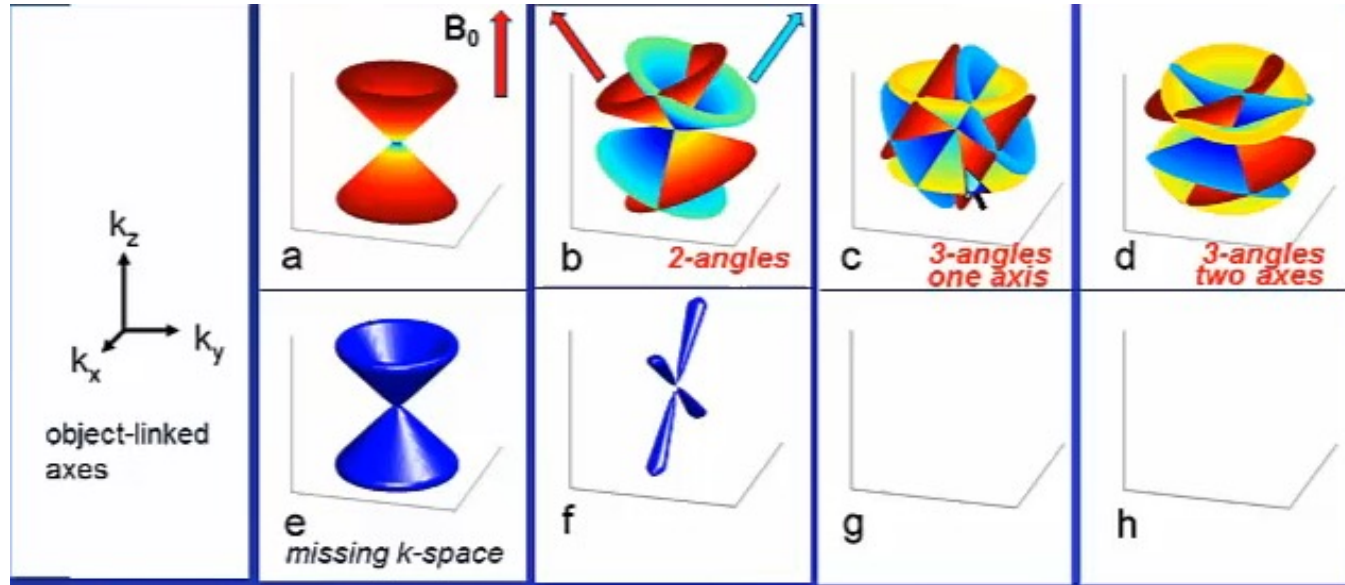
QSM - Dipole Inversion

COSMOS: calculation of susceptibility using multiple orientation sampling



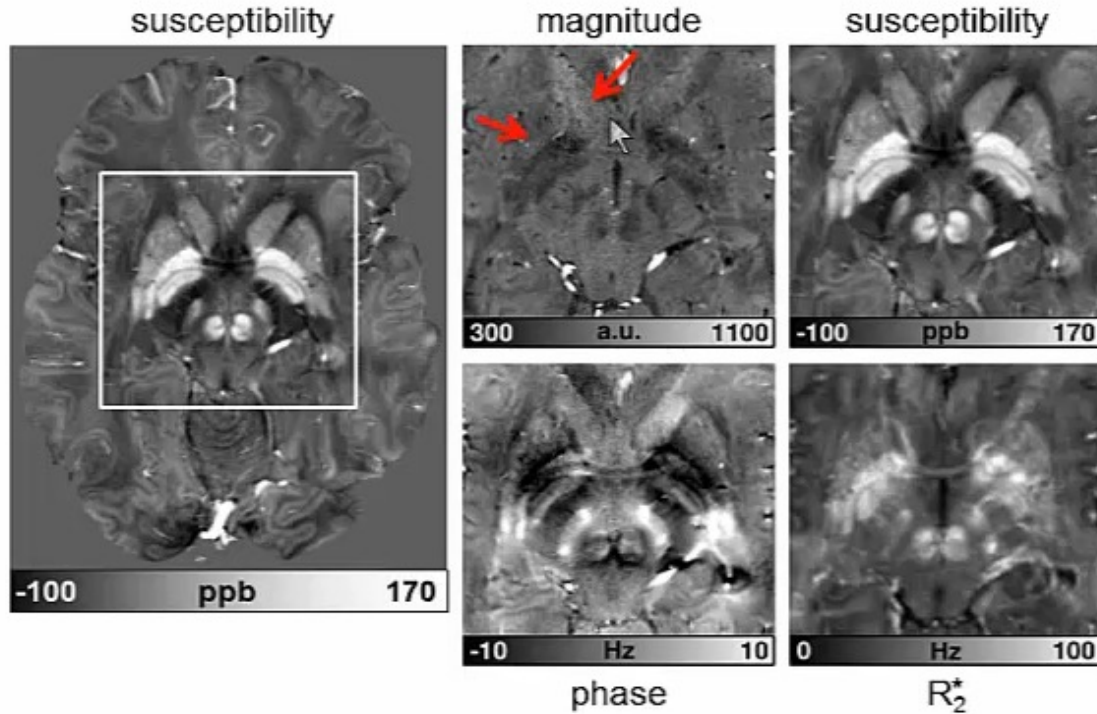
QSM - Dipole Inversion

COSMOS: calculation of susceptibility using multiple orientation sampling



QSM - Dipole Inversion

COSMOS:



Deistung, A et al. *NeuroImage* 2013, 65, 299–314.

QSM Dipole Inversion: iLSQR

iLSQR: iterative method solving least square using the orthogonal and right triangular decomposition

Dipole kernel

$$\psi(\mathbf{k}) = D_2(\mathbf{k}) \cdot \chi(\mathbf{k})$$

Field perturbation

Susceptibility distribution

1st order derivative

$$\psi'(\mathbf{k}) + [2(k_x^2 + k_y^2)k_z/k^4] \cdot \chi(\mathbf{k}) - D_2(\mathbf{k}) \cdot \chi'(\mathbf{k}) = 0$$

$$D_3(\mathbf{k}) \cdot \chi(\mathbf{k}) + D_2(\mathbf{k}) \cdot FT[i \cdot r_z \chi(\mathbf{r})] = FT[i \cdot r_z \psi(\mathbf{r})]$$


$$\chi(\mathbf{k}) = D_2(\mathbf{k})^{-1} \cdot \psi(\mathbf{k}), \text{ when } D_2(\mathbf{k}) \geq \varepsilon$$

$$\chi(\mathbf{k}) \approx D_3(\mathbf{k})^{-1} \cdot FT[ir_z \psi(\mathbf{r})], \text{ when } D_2(\mathbf{k}) < \varepsilon$$

Where: $D_3(\mathbf{k}) = (k_x^2 + k_y^2)k_z/\pi k^4$.

QSM Dipole Inversion: iterative inversion methods with regularization

Recon problem

$$\operatorname{argmin}_x \frac{1}{2} \left\| W(F^H D F \chi - \Phi) \right\|_2^2 + \alpha \Omega(\chi)$$

Data consistency term

Regularization term

Nonlinear variant

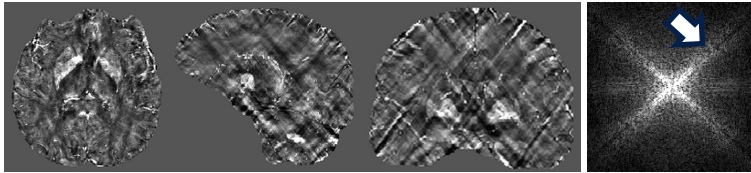
$$\operatorname{argmin}_x \frac{1}{2} \left\| W \left(e^{iF^H D F \chi} - e^{i\Phi} \right) \right\|_2^2 + \alpha \Omega(\chi)$$

Method	Data consistency term	Regularization term
STAR-QSM (STreaking Artifact Reduction for QSM)	Linear L2-norm	Total variation
FANSI (FAst Nonlinear Susceptibility Inversion)	Nonlinear L2-norm	Total variation
HD-QSM (Hybrid Data fidelity)	Linear L1+L2-norm	Total variation
MEDI (Morphology Enabled Dipole Inversion)	Linear L1-norm	L1 norm of morphologically weighted gradients

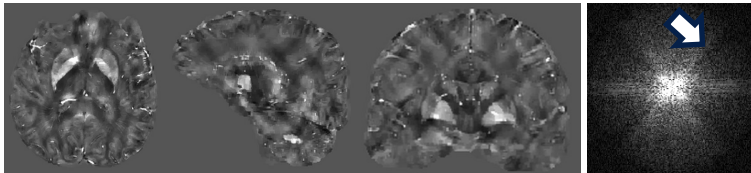
QSM Dipole Inversion: iterative inversion methods with regularization

Parameter optimization

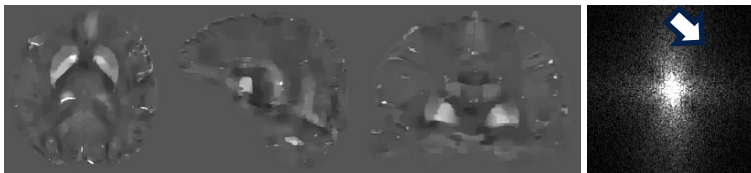
(A) $\lambda = 10^{-6}$



$\lambda = 10^{-4.2}$

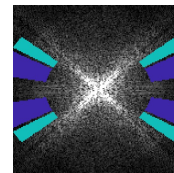
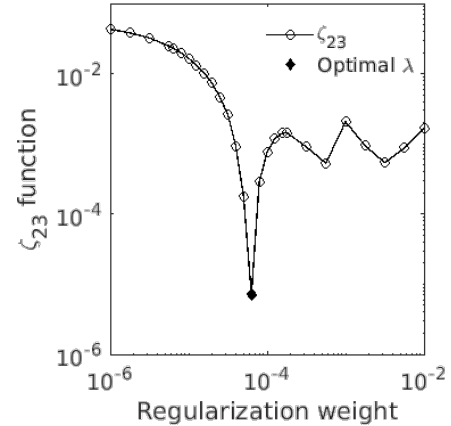


$\lambda = 10^{-3.5}$



(B)

Frequency Equalization Plot



■ M2 $\xi_{ij} = \left(\frac{A_i - A_j}{A_i + A_j} \right)^2$
■ M3 A_i : Mean power in M_i

QSM Dipole Inversion: single step methods

QSIP

Quantifying Susceptibility by Inversion of a Perturbation model

$$\chi_1^* = \arg \min_{\chi_1} \left[\lambda_1 \|W \circ (\Delta B - \Delta (K_s * \chi_1))\|_1 + \lambda_2 \|M \circ (B - (K_s * \chi_1 + B_e))\|_2^2 + \lambda_3 \|M^C \circ (\chi_1 + \chi_0 / \delta)\|_2^2 \right]$$

Simultaneously estimating the external susceptibility outside the brain

SSTV, SSTGV

Single Step QSM with Total Variation / Total Generalized Variation penalties

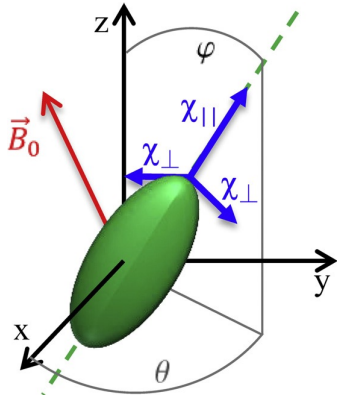
$$\min_{\chi} \frac{1}{2} \sum_i \left\| |M_i F^{-1} H_i D F \chi - M_i F^{-1} H_i F \Psi(\phi)| \right\|_2^2 + R(\chi)$$

Perform VSHARP background field removal and dipole inversion in a single step

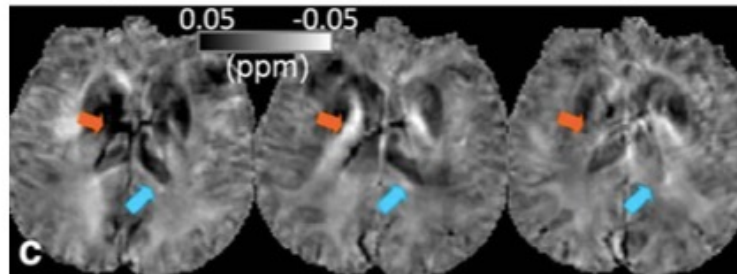
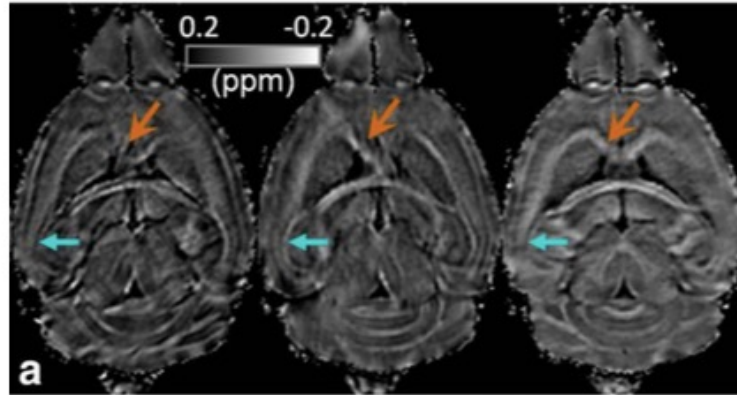
QSM: Anisotropic Susceptibility

$$\underline{\underline{M}} = \underline{\underline{\chi}} \underline{\underline{H}}$$

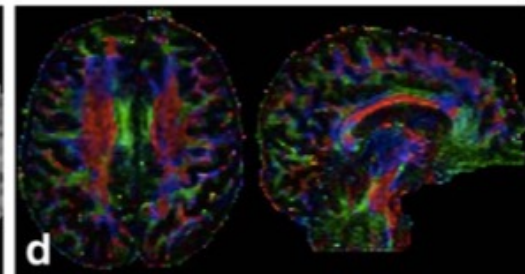
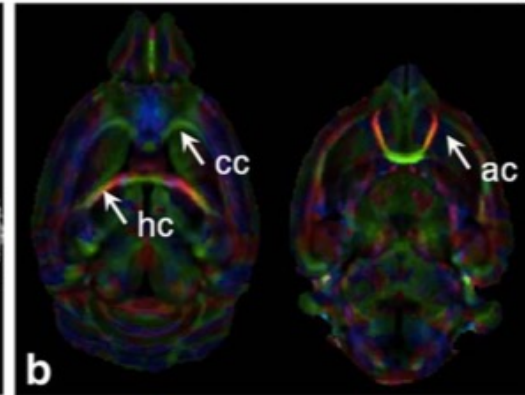
$$\underline{\underline{\chi}} = \begin{bmatrix} \chi_{11} & 0 & 0 \\ 0 & \chi_{22} & 0 \\ 0 & 0 & \chi_{33} \end{bmatrix}$$



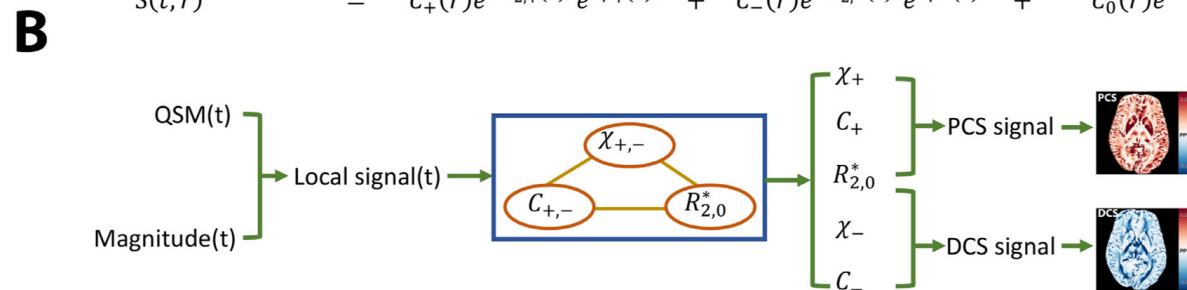
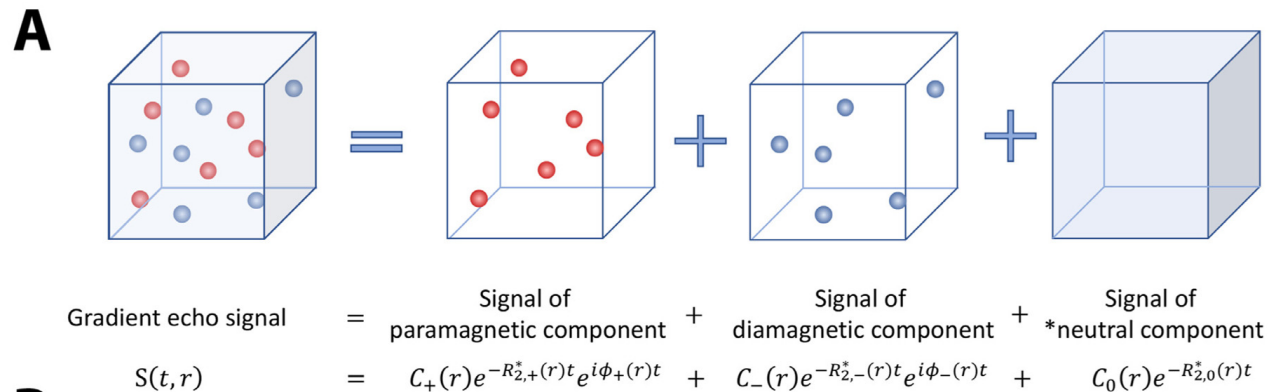
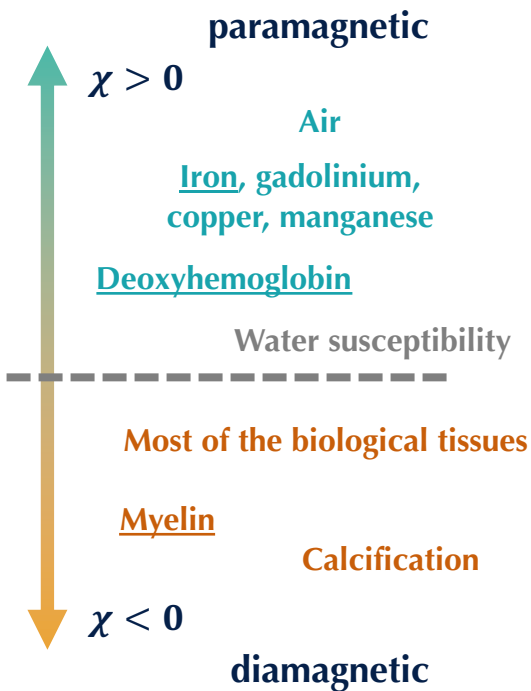
Susceptibility Anisotropy



Susceptibility Tensor Imaging

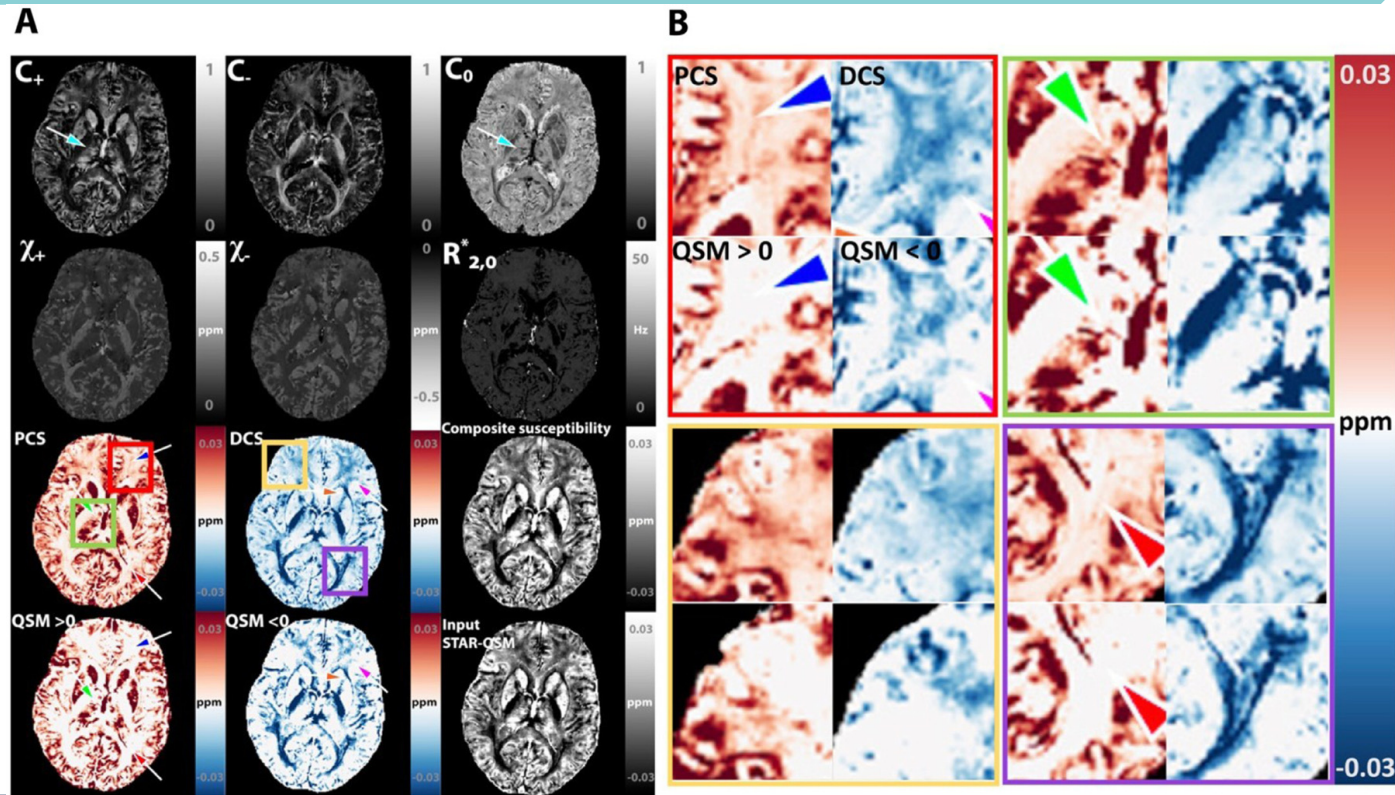


QSM: Susceptibility source decomposition



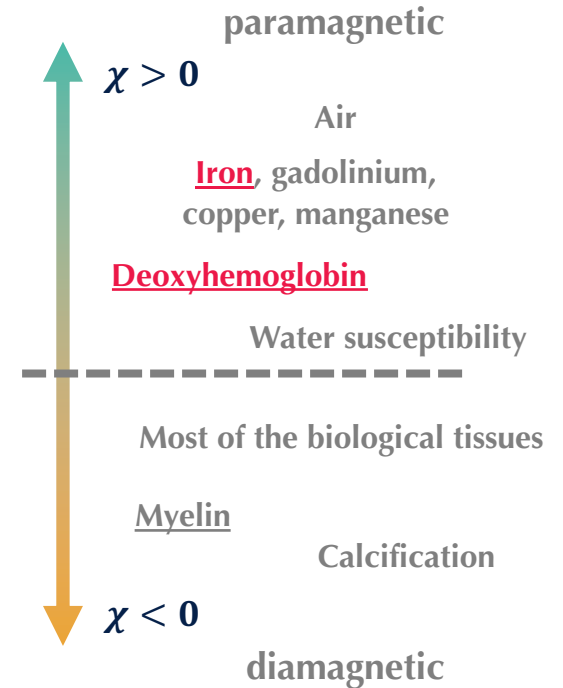
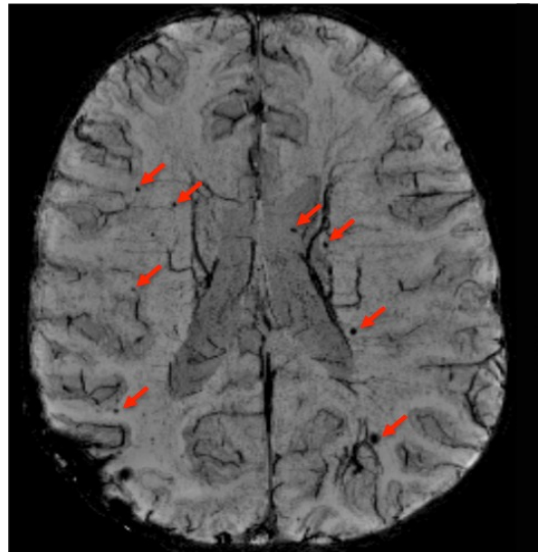
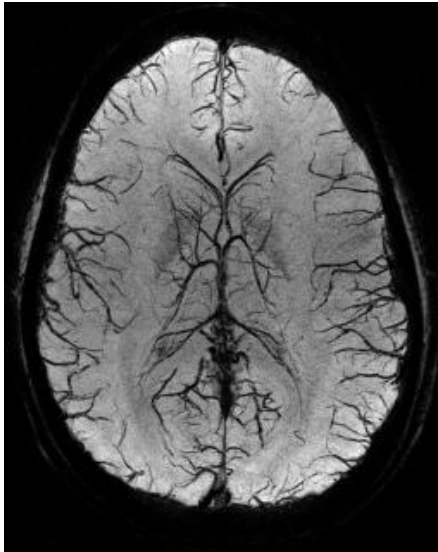
*neutral component means the component is susceptibility neutral relative to the susceptibility reference.

QSM: Susceptibility source decomposition



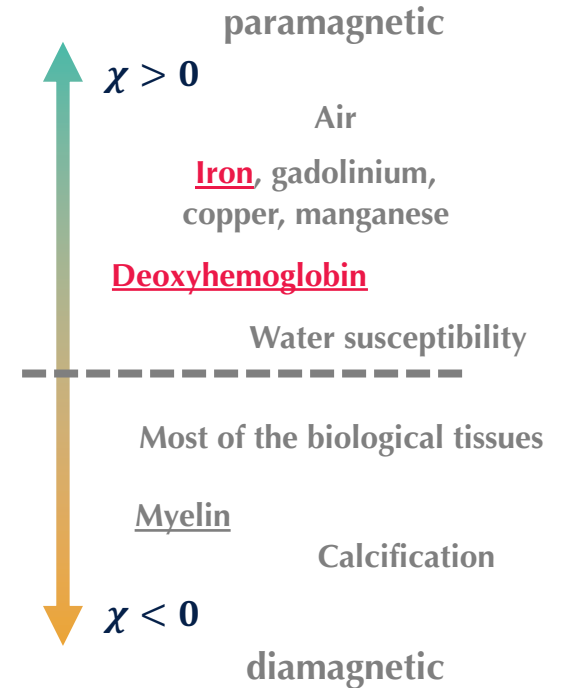
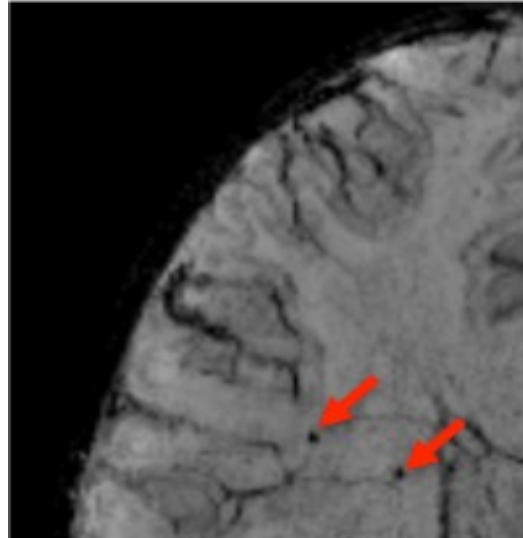
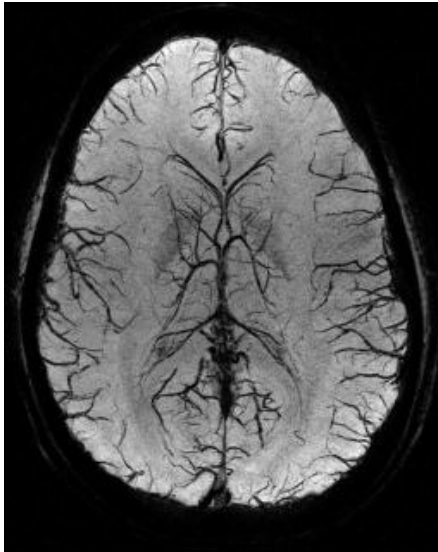
Susceptibility MRI – SWI

phase-weighted magnitude imaging



Susceptibility MRI – SWI

phase-weighted magnitude imaging



SWI – Processing

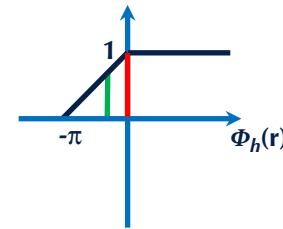
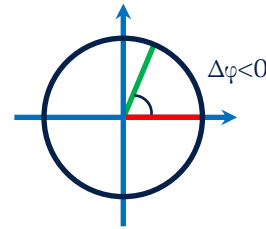
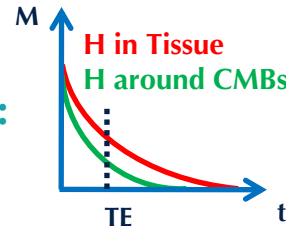
Contrast:

Magnitude

Phase

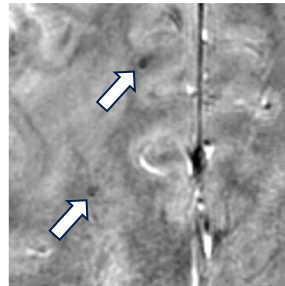
SWI

Effect of $\Delta\chi$:

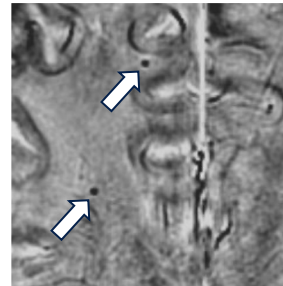


Accumulates phase

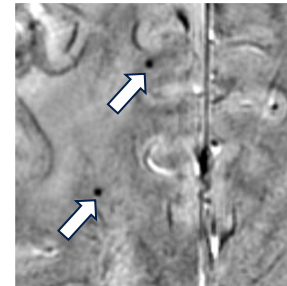
Enhances $T2^*$
shortening



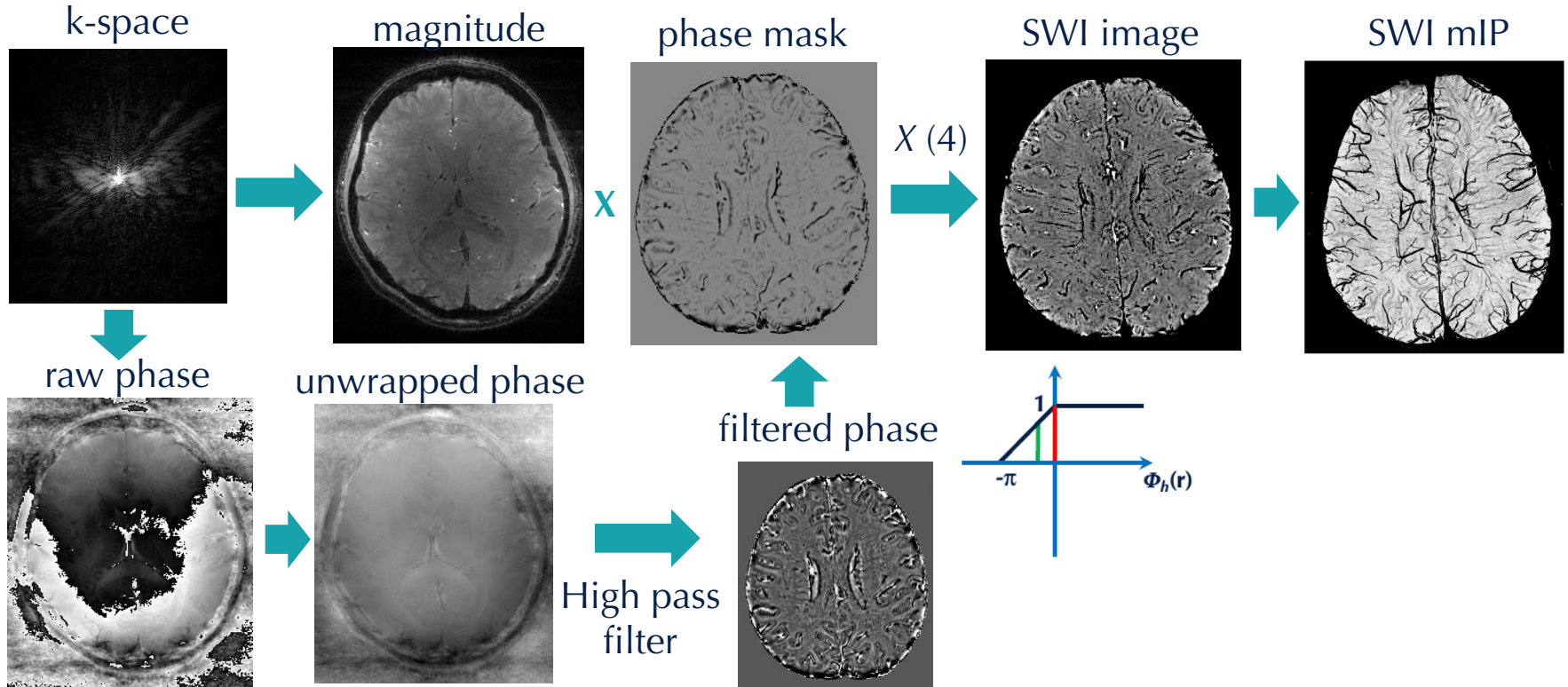
+



→

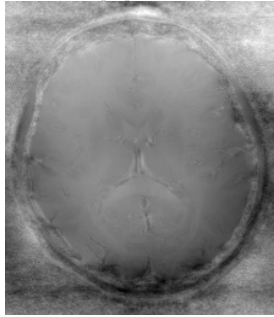


SWI – Processing



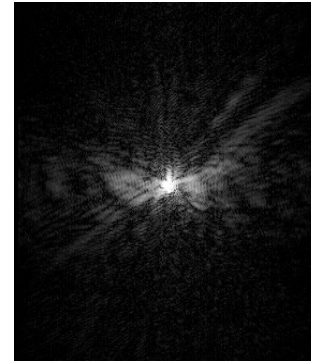
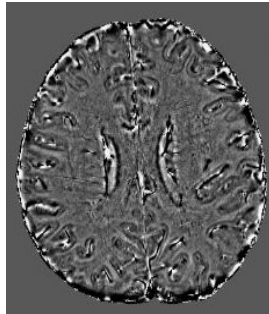
SWI – Processing

unwrapped phase

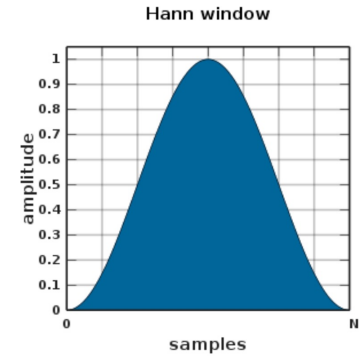


High pass filter

filtered phase



X

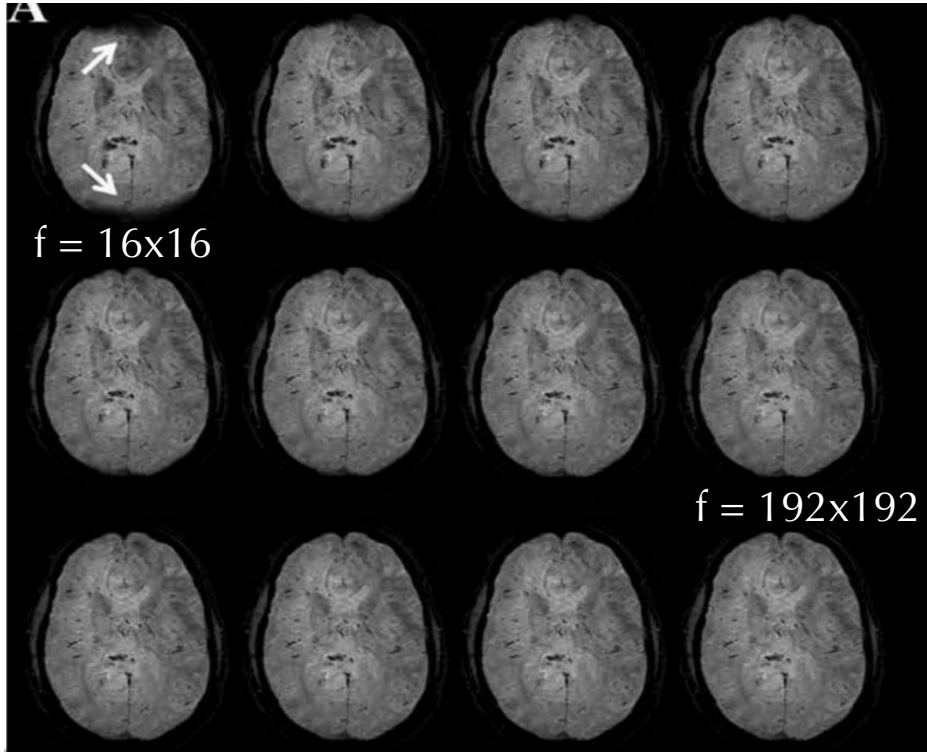
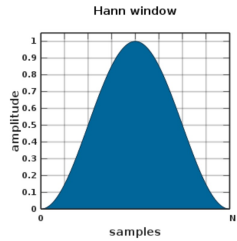


Low pass filtered phase

Complex division



SWI – Processing

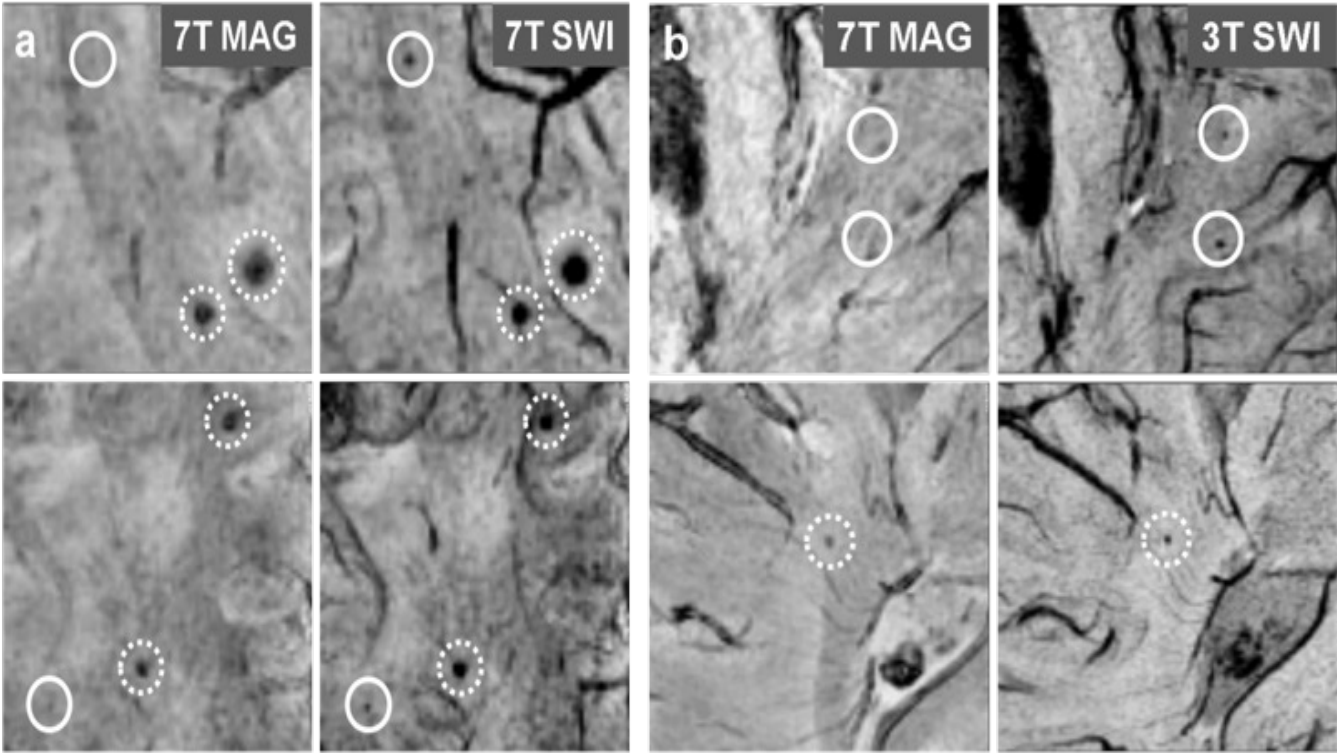


Higher contrast,
more artifacts



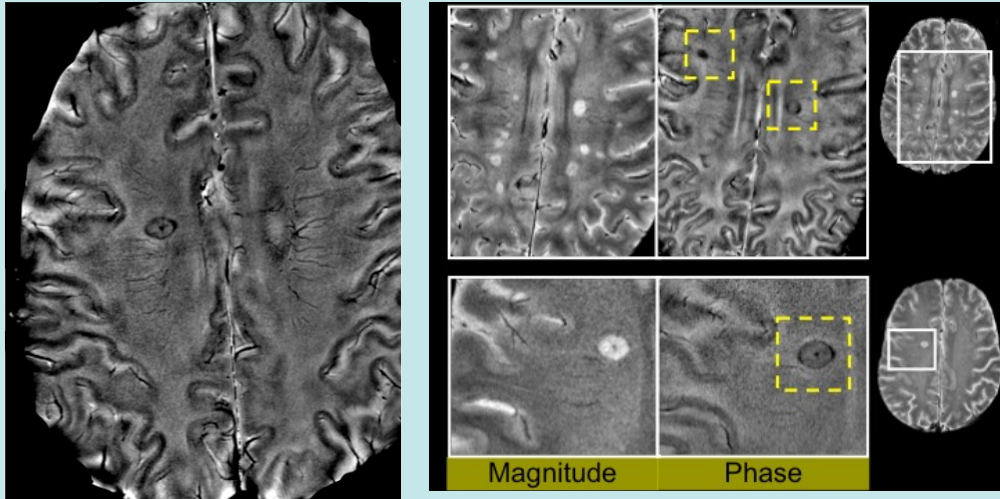
lower contrast,
less artifacts

SWI at 7T

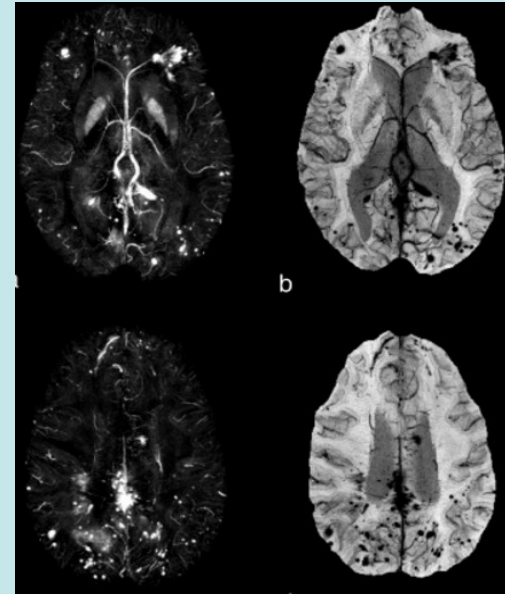


QSM/SWI – Clinical applications

Multiple Sclerosis

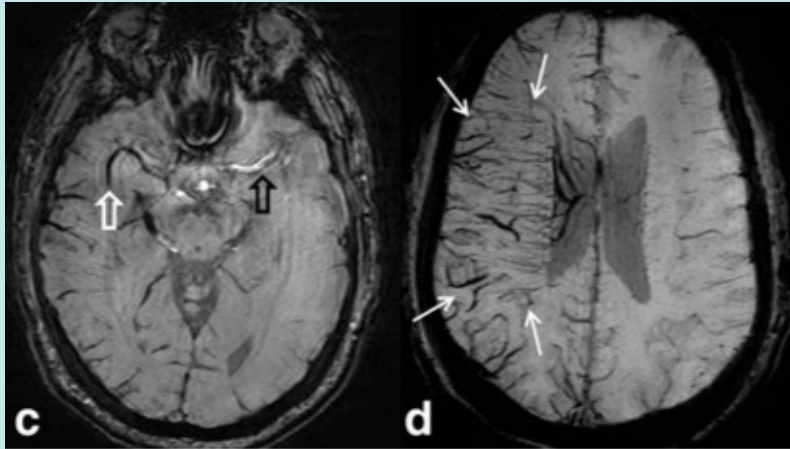


Traumatic Brain Injury

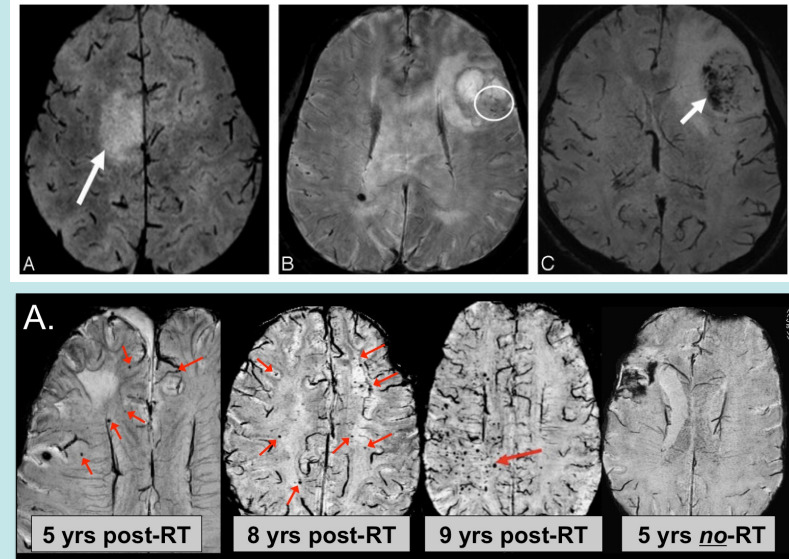


QSM/SWI – Clinical applications

Stroke

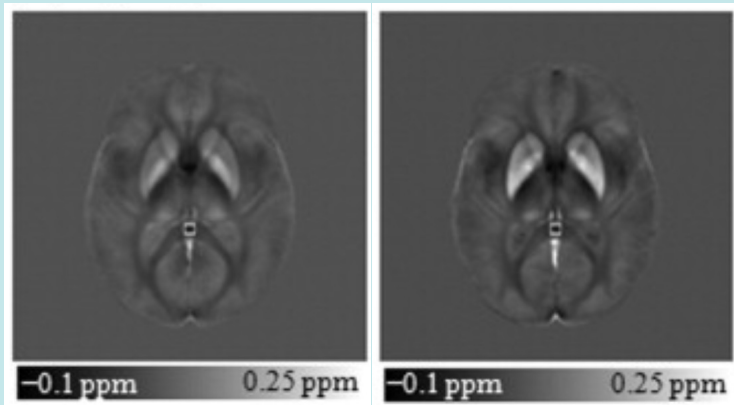


Brain Tumor



QSM/SWI – Clinical applications

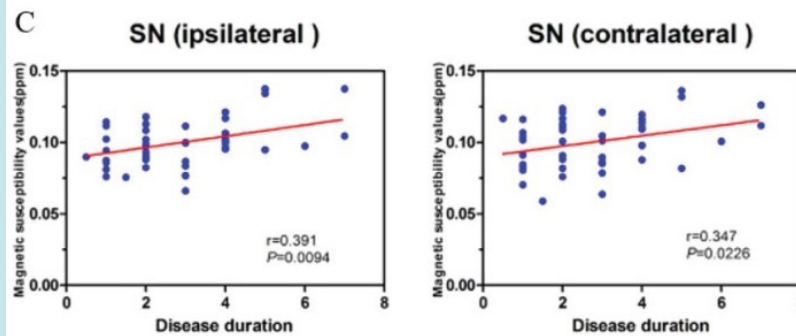
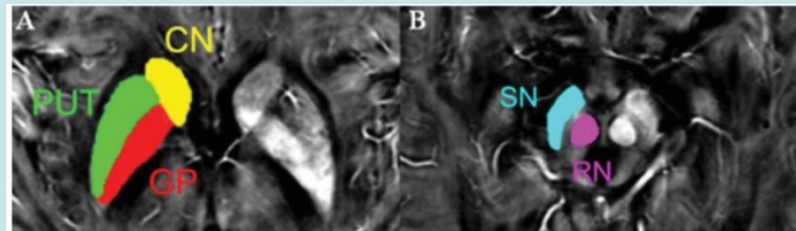
Aging



Young

Elderly

Parkinson's Disease



Conductivity imaging (Electrical Properties Tomography)

- **Electrical conductivity (σ)**: the ability of a material to transport charges, or equivalently, to carry an electric current.
- **Electrical permittivity (ϵ)**: the ability of a material to rotate molecular dipoles and trap/store charge; hence the degree to which a material becomes polarized when placed in an electric field.

Helmholtz equation

$$-\nabla^2 \mathbf{H} = \frac{\nabla \kappa}{\kappa} \times [\nabla \times \mathbf{H}] + \omega^2 \mu \kappa \mathbf{H},$$

H: Magnetic Field
 κ : complex permittivity
 $= \epsilon - i(\sigma/\omega)$
 μ : magnetic permeability

Conductivity imaging

$$-\nabla^2 \mathbf{H} = \frac{\nabla \kappa}{\kappa} \times [\nabla \times \mathbf{H}] + \omega^2 \mu \kappa \mathbf{H},$$



Piecewise constant κ
Constant μ

$$\kappa(\mathbf{r}) = \frac{-1}{\omega^2 \mu_0} \frac{\nabla^2 H^+(\mathbf{r})}{H^+(\mathbf{r})},$$

$$\sigma = \frac{1}{\omega \mu_0} \text{Im} \left\{ \frac{\nabla^2 H^+}{H^+} \right\}, \quad \epsilon = \frac{-1}{\omega^2 \mu_0} \text{Re} \left\{ \frac{\nabla^2 H^+}{H^+} \right\}$$

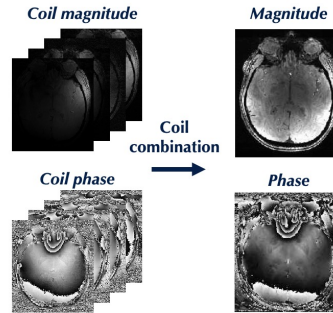
Simplified H-EPT

$$\sigma = \frac{1}{\omega \mu_0} \nabla^2 \hat{\phi}^+$$

Conductivity imaging

Simplified H-EPT/
phase-based EPT

$$\sigma = \frac{1}{\omega\mu_0} \nabla^2 \hat{\phi}^+$$



Measured phase
(single coil)

$$\begin{aligned} \phi(\vec{r}, TE) \\ = \phi_0(\vec{r}) + \phi_{total}(\vec{r}, TE) \end{aligned}$$



$$\phi_0 = \phi^+ + \phi^-$$

$$\phi^+ \approx \tilde{\phi}_0/2 = (\phi^+ + \tilde{\phi}^-)/2$$

Transceive phase assumption

Transceive phase

Conductivity imaging

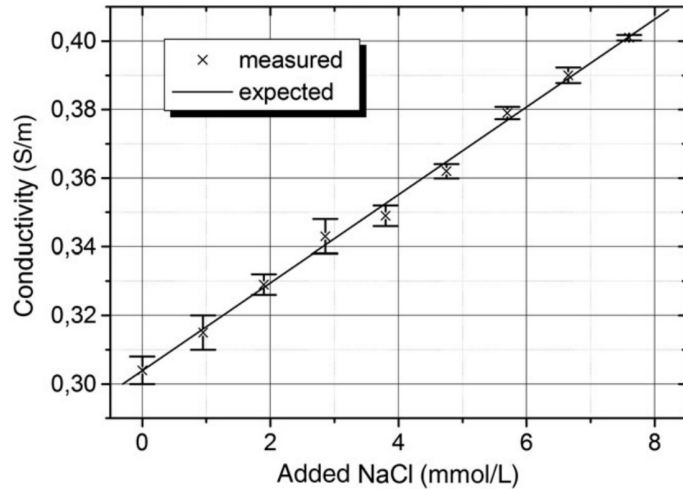
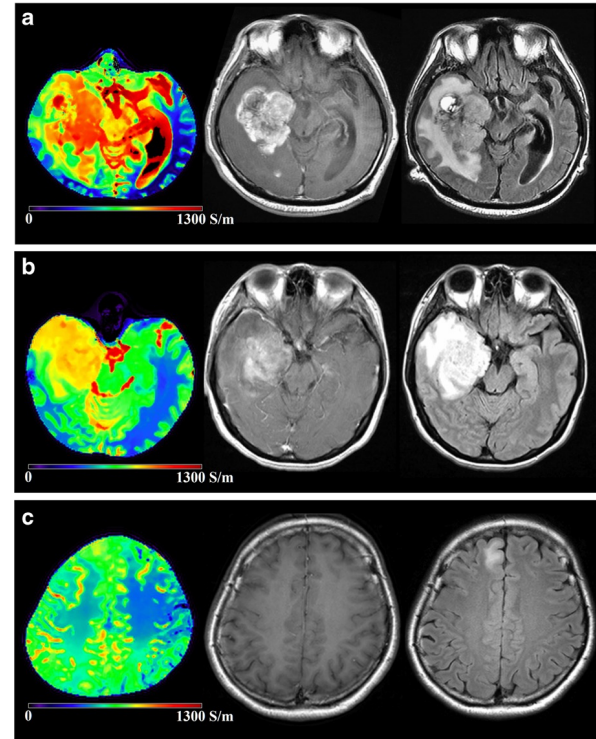


FIGURE 4 Electrical properties tomography (EPT) phantom measurements at different saline concentrations. The plot clearly shows the different steps of added NaCl, corresponding to an accuracy of about 10 mS/m. Error bars indicate standard deviation over the averaged 50×50 voxels in the center of the phantom



REVIEW ARTICLE

Electric properties tomography: Biochemical, physical and technical background, evaluation and clinical applications

Ulrich Katscher¹  | Cornelius A.T. van den Berg²

¹Department of Tomographic Imaging, Philips Research Laboratories, Hamburg, Germany

²Department of Radiotherapy, University Medical Center, Utrecht, the Netherlands

Correspondence

U. Katscher, Department of Tomographic Imaging, Philips Research Laboratories, Roentgenstrasse 24–26, 22335 Hamburg, Germany.

Email: ulrich.katscher@philips.com

Electric properties tomography (EPT) derives the patient's electric properties, i.e. conductivity and permittivity, using standard magnetic resonance (MR) systems and standard MR sequences. Thus, EPT does not apply externally mounted electrodes, currents or radiofrequency (RF) probes, as is the case in competing techniques. EPT is quantitative MR, i.e. it yields absolute values of conductivity and permittivity. This review summarizes the physical equations underlying EPT, the corresponding basic and advanced reconstruction techniques and practical numerical aspects to realize these reconstruction techniques. MR sequences which map the field information required for EPT are outlined, and experiments to validate EPT in phantom and *in vivo* studies are described. Furthermore, the review describes the clinical findings which have been obtained with EPT so far, and attempts to understand the physiologic background of these findings.

KEYWORDS

electric conductivity, EPT, numerical differentiation, permittivity, tumor characterization